NASA
Technical
Paper
2723

August 1987

Calibration of the Spin-Scan Ozone Imager Aboard the Dynamics Explorer 1 Satellite

Walter E. Bressette,
Gerald M. Keating,
and David F. Young

NASA

NASA
Technical
Paper
2723

1987

Calibration of the Spin-Scan Ozone Imager Aboard the Dynamics Explorer 1 Satellite

Walter E. Bressette
and Gerald M. Keating
Langley Research Center
Hampton, Virginia

David F. Young
ST Systems Corporation (STX)
Hampton, Virginia

National Aeronautics
and Space Administration

**Scientific and Technical
Information Office**

Contents

Acknowledgment

We wish to thank all members of the Dynamics Explorer Auroral Imager Project Office at the University of Iowa for their efforts in obtaining and sending to the Langley Research Center the basic DE-1 total ozone data used in this report, in particular, L. A. Frank, J. D. Craven, K. L. Ackerson, and M. R. Dvorsky.

This report would not have been possible without the efforts of P. K. Bhartia, D. Gordon, and others of ST Systems Corporation (STX) under NASA Contracts NAS1-15785 and NAS1-17089. Dr. Bhartia played an important role in devising the total ozone algorithm, performing the early theoretical calculations, and developing the computer programs for determining total ozone data from the DE-1 radiance data.

Abstract

This paper presents the calibration technique, contains calculated backscattered radiance values necessary for performing the calibrations, and provides the calibration constants for September–October 1981 to determine total columnar ozone from the Spin-Scan Ozone Imager (SOI), which is a part of the auroral imaging instrumentation aboard the Dynamics Explorer 1 satellite. The precision of the SOI derived total columnar ozone is estimated to be better than 2.4 percent. Linear regression analysis was used to calculate correlation coefficients between total columnar ozone obtained from Dobson ground stations and SOI which indicate that the SOI total columnar ozone determination is equally accurate for clear or cloudy weather conditions.

Introduction

The Dynamics Explorer 1 spacecraft (DE-1), with instrumentation designed by the University of Iowa for obtaining global images of the auroral oval, was determined to be a suitable spacecraft for obtaining large-scale synoptic images of the Earth's total ozone field. For the experiment, optical filters at 317.5 and 360 nm were added to the filter wheels of two of the three imaging photometers on DE-1. These optical filters used in conjunction with the spin of DE-1 and the varying position of scanning mirrors in the photometers constitute an ozone mapping system designated the Spin-Scan Ozone Imager (SOI) (ref. 1). Since the SOI system does not have an internal calibration source, in-flight calibration of the system must be obtained by other means, such as by comparison with Dobson ground station total ozone measurements.

DE-1 was launched into Earth orbit on August 3, 1981. Because of the highly eccentric orbit of DE-1 (apogee 23 300 km, perigee 550 km) and the excellent resolution of the University of Iowa imaging instrumentation (ref. 2), a detailed synoptic total ozone map of a large continental-scale area has been obtained every 12 minutes for several consecutive hours on many days from the higher portions of the orbit. At the lower altitudes, smaller scale, higher spatial resolution ozone maps have been produced.

The main purpose of this paper is to provide the SOI calibration constants for determining total columnar ozone for September–October 1981 and to provide the information for updating the calibration of SOI through 1986. This paper also includes (1) a discussion of the total columnar ozone satellite measurement technique, (2) a brief description of the instrumentation on DE-1 that applies to SOI, (3) a discussion of the SOI calibration technique that utilizes Dobson ground station total columnar ozone data to obtain the calibration, (4) the calculated backscattered radiance values at 317.5 and 360 nm that are used to perform the SOI calibration, and (5) a compilation of the days that SOI Earth radiance data were obtained from September 1981 to June 1984.

Symbols

a_λ	atmospheric albedo
B	angular surface brightness, 10^6 photons/cm^2-sec-sr
C_λ	photometer-detected energy, counts/pixel
$\overline{C}_\lambda$	average photometer-detected energy, hourly counts from a 6° latitude × 6° longitude pixel box divided by number of pixels in the box
c	velocity of light, 3×10^8 m/sec
dA	unit area or area of pixel
dw	solid angle
E	energy, joules/photon
F_λ	solar flux, watts/cm^2
$\overline{F}_\lambda$	average solar flux over optical-filter bandwidth, watts/cm^2-cm
h	Planck's constant, 6.63×10^{-34} joule-sec
I_λ	solar flux diffusely scattered into a hemisphere in a direction θ from $I_{\lambda,n}$, and an azimuth angle ϕ from the direction of F_λ per unit time, per unit frequency, per unit solid angle, watts/cm^2-sr
$\overline{I}_\lambda$	average backscattered radiance over optical-filter bandwidth, watts/cm^2-cm-sr
$I_{\lambda,n}$	solar flux diffusely scattered perpendicular to a unit area into a hemisphere per unit time, per unit frequency, per unit solid angle, watts/cm^2-sr
K	317.5-nm conversion factor
N	SOI scan line number
R	reflectivity from underlying surface (clouds, ground, water)
S_λ	photometer sensitivity, counts/kRa-pixel-T_λ

$\overline{S}_\lambda$ photometer sensitivity averaged over bandwidth of optical filter, counts/kRa-pixel

s average relative slant path (calculated for an average value of Ω (300 D.U.) at $R = 0.10$)

T_λ transmission at a given wavelength

$\overline{T}_\lambda$ average transmission over optical-filter bandwith

W_λ calibration factor, $C_\lambda / \overline{I}_\lambda$

y $= \sec\theta_0 + \sec\theta$

α ozone absorption coefficient, $(\text{atm-cm})^{-1}$

θ angle between the viewing direction and the perpendicular at the pixel, deg

$\overline{\theta}$ hourly average of θ at a given location, deg

θ_0 angle between the altitude of the Sun and the perpendicular at the pixel or unit area, deg

$\overline{\theta}_0$ hourly average of θ_0 at a given location, deg

λ wavelength, nm or Å

ϕ angle between two planes that pass through the center of the Earth, one plane containing the Sun and the observation pixel and the other one containing θ, deg

$\overline{\phi}$ hourly average of ϕ at a given location, deg

Ω total columnar ozone, D.U.

Subscripts:

1 wavelength of 317.5 nm

2 wavelength of 360.0 nm

c calculated data

co calculated data in the absence of ozone

λ wavelength dependent

Abbreviations:

DE-1 Dynamics Explorer 1

D.U. Dobson unit, 10^{-3} atm-cm

Ra rayleigh, 10^6 photons/cm^2-sec, reported in terms of $4\pi B$ sr

SOI Spin-Scan Ozone Imager

Total Columnar Ozone Measurement Concept

The algorithm used to determine total columnar ozone (Ω) from the SOI measurement of backscattered ultraviolet (BUV) radiance was derived from the BUV technique discussed in references 3, 4, 5, and 6. In the SOI experiment, a backscattered solar radiance is measured at the wavelength of 317.5 nm. That radiation passed down through the atmospheric ozone (O_3), which is concentrated mainly in the stratosphere, was backscattered primarily in the troposphere below the O_3, and then passed back through the O_3 to the satellite. To determine Ω, the backscattered radiance that was attenuated by O_3 during both passes through the atmosphere is first converted to an atmospheric albedo and then compared with a Lambertian atmospheric albedo at 317.5 nm which was calculated theoretically for an ozone-free atmosphere.

Atmospheric Albedo

Referring to figure 1, where F_λ is the solar flux and θ_0 the solar zenith angle, $F_\lambda \cos\theta_0$ is the component of solar energy flux reflected into a hemisphere whose equatorial plane is along the underlying reflecting surface that contains unit area dA. Thus an increment of reflected incident energy Q is

$$dQ = F_\lambda \cos\theta_0 \, dA \, dt \, d\lambda \tag{1}$$

For a perfect Lambertian reflecting surface, I_λ is that portion of dQ that is reflected within the solid angle dw in a direction that makes an angle θ with the normal to dA and in an azimuthal direction defined by the angle ϕ. Then

$$I_{\lambda,n} = \frac{I_\lambda}{\cos\theta} \tag{2}$$

defines the component of I_λ reflected diffusely back into the hemisphere in the direction normal to dA per unit area, per unit time, per unit wavelength, and per unit solid angle. For each increment of energy dQ, integration of I_λ over the solid angle dw of the hemisphere yields

$$F_\lambda \cos\theta_0 = \int I_{\lambda,n} \cos\theta \, dw = \int_0^{2\pi} \int_0^{\pi/2} I_{\lambda,n} \cos\theta \sin\theta \, d\theta \, d\phi \tag{3}$$

since $dw = \sin\theta\ d\theta\ d\phi$. For the perfect Lambert reflector, $I_{\lambda,n}$ is independent of direction and the integration in equation (3) results in

$$F_\lambda \cos\theta_0 = \pi I_{\lambda,n} \tag{4}$$

Now defining the atmospheric albedo as

$$a_\lambda = \frac{I_\lambda(\theta_0, \theta, \phi)}{I_{\lambda,n}} \tag{5}$$

and substituting from equation (4) gives

$$a_\lambda = \frac{\pi I_\lambda(\theta_0, \theta, \phi)}{F_\lambda \cos\ \theta} \tag{6}$$

Reflectivity

In reference 7, it is shown that I_λ contains two radiance terms: atmospheric backscattered radiance (I_0), which is unaffected by a surface reflection (R) (land, water, clouds); and a component which accounts for the direct and the diffused radiation resulting from R. Thus, in an ozone-free atmosphere,

$$I_\lambda(\theta_0, R) = I_0(\theta_0, 0) + \frac{T_a(\theta_0)R}{1 - RS_b} \tag{7}$$

where

$I_\lambda(\theta_0, R)$	backscattered radiance for conditions specified by θ_0 and R
$I_0(\theta_0, 0)$	backscattered radiance for conditions specified by θ_0 and $R = 0$
$T_a(\theta_0)$	extraterrestrial irradiance times the incoming and outgoing transmittances
S_b	fraction of the reflected radiation scattered back by the atmosphere from isotropically reflected surface radiation

Therefore, for constant $F_\lambda \cos\theta$ in equation (6), a_λ differs for different values of R, since I_λ in equation (7) is a function of R.

In the SOI experiment, R is determined from backscattered radiance measured outside the O_3 absorption band at the wavelength of 360 nm (I_2). The SOI-measured value of I_2 is converted to a 360-nm atmospheric albedo (a_2) using equation (6), and the value of R at 360 nm is then obtained from values derived from radiation transfer calculations of 360-nm atmospheric albedo ($a_{2,c}$) versus R at the appropriate values of θ_0, θ, and ϕ, after assuming that a_2 equals $a_{2,c}$.

SOI Algorithm

In considering the passage of ultraviolet solar radiation through the upper atmosphere, as is the case in the SOI experiment, both scattering and emission of the radiation can be neglected. In reference 8, it is shown that atmospheric attenuation of radiance over a distance where only absorption exists is an exponential function of both the absorption coefficient and the density of the atmospheric medium. These results are applied in the SOI algorithm as follows:

$$a_1 = a_{1,co} e^{-\alpha\Omega(\sec\theta_0 + \sec\theta)} \tag{8}$$

where

a_1	observed atmospheric albedo at 317.5 nm
$a_{1,co}$	calculated atmospheric albedo at 317.5 nm for an ozone-free atmosphere
α	ozone absorption coefficient at 317.5 nm
Ω	total columnar ozone

The path length relative to the vertical distance through the ozone layer is $\sec\theta_0 + \sec\theta$. The operational expression for determining Ω from SOI data resulting from equation (8) is

$$\Omega = \frac{1}{\alpha s} \ln \frac{a_{1,co}}{a_1} \tag{9}$$

where $a_{1,co}$ is obtained from values calculated from radiation transfer theory of $a_{1,co}$ versus R as a function of θ_0, θ, and ϕ, after assuming that R at 360 nm obtained from I_2 has the same value at the wavelength of 317.5 nm. This assumption is considered valid, because the high values of R result from reflection from white clouds that generally have uniform spectral reflectivity while the variable reflectivity surface features (which as seen in ref. 9 can vary between 317.5 and 360 nm by as much as 20 percent) have values of R at both wavelengths of less than 10 percent and, therefore, do not contribute appreciably to the backscattered radiance at either wavelength. The parameter s is the relative slant path calculated as a function of $\sec\theta_0 + \sec\theta$ for an average mid-Northern-Hemisphere latitude value of Ω of 300 D.U. The parameter s accounts for changes

in the backscattered radiance and path length due to variations in θ_0 and θ. The values of s are obtained by a curve fit to y as shown in the results section of this paper. Finally, SOI radiance data at 317.5 nm are converted to a_1 using conversion factors obtained, as explained in the results and discussion section of this paper, during an in-flight calibration period where Dobson station total ozone data are used in equation (9).

Instrumentation

A sketch of the DE-1 spacecraft is presented in figure 2. The satellite with its spin axis perpendicular to its orbital plane spins at approximately 10 revolutions per minute. DE-1 contains three imaging photometers whose optical axes are located in the orbital plane as shown in figure 3. Visible photometers A and B, used in the SOI experiment, have their fields of view separated by 120°.

The Pixel Array

Each photometer has a 0.32° conical field of view. The instrument scan mirror is rotated in 0.25° increments orthogonal to the orbital plane to control the direction of the field of view. The full scan angle of the scanning mirror is limited to 30°, 15° on each side of the orbital plane, and its axis is centered perpendicular to the spin axis. The stepwise rotation of the scanning mirror and the spacecraft rotation are used to develop a scene composed of a two-dimensional pixel array. The 30° angular width scene is obtained from 120 spacecraft rotations during 12 minutes. The incremental rotation of the instrument scanning mirror is synchronized with the spacecraft rotation by nadir pulses obtained from infrared horizon sensors on the spacecraft, and the time-dependent relative phase of the pixels from rotation to rotation is determined from the spacecraft aspect sensors. Additional details concerning the formation of scenes from the photometer pixel array are discussed in reference 2.

As an indication of scene location accuracy, figure 4 shows a comparison of the location of cloud edges measured from SOI scenes with the location of the same cloud edges measured from Geostationary Operational Environmental Satellite (GOES) scenes on October 2, 1981. It is seen in figure 4 that the cloud locations measured from the two satellite scenes lie within ±1° of each other. Thus, it is evident that the pixel location system for DE-1 is not a limiting factor for producing ozone maps to a spatial accuracy of ±1°.

Principal Optical Elements

The principal optical elements of a DE-1 photometer are displayed in the schematic of figure 5. These elements are a baffled aperture for minimizing the solid angle of the Earth's reflected sunlight as seen at the stepping mirror, the stepping mirror for selecting the direction of the solid angle field of view, and a parabolic mirror for focusing the solid angle on the pinhole of the focal-plane optical assembly. The 1130-μm-diameter pinhole, a $f/1.7$ collimating lens, a filter wheel and its drive motor, and a photomultiplier tube comprise the focal-plane optical assembly. The $f/1.7$ collimating lens is necessary to reduce the loss of sensitivity due to pinhole beam divergence through the narrow-bandwidth filters used in the SOI experiment. For the SOI experiment discussed in this paper, a 317.5-nm narrow-bandwidth filter is mounted on the filter wheel of photometer B, and a 360-nm narrow-bandwidth filter is included in the filter complement of photometer A.

Preflight Calibration

Optical Filters

Measurements of the wavelength dependence of transmission for the 317.5- and 360-nm optical filters were made by T. Pepin at the University of Wyoming. The measurements, plotted in figure 6, were obtained over 0.3-nm wavelength increments using a holographic grating monochromator system that was built for studying in-band and out-of-band characteristics of interference filters. The filters, as seen in figure 6, are by definition narrow-bandwidth filters, because they have bandwidths at 50 percent of their peak transmission of approximately 1 percent of their central wavelength. The very low peak transmission values, resulting from the use of neutral density filters, were required to avoid visible radiation saturation damage to the highly sensitive photometer system, designed for dark background aurora imaging, when measuring ozone on the sunlit side of the Earth. The peak transmission value for the 360-nm filter has been attenuated by approximately a factor of 2 more than the value for the 317.5-nm filter.

The average transmission $(\overline{T}_\lambda)$ for the 317.5- and 360-nm SOI optical filters was obtained by integrating the area under the measured transmission curves in figure 6 over the wavelength region bounded by the transmission values at 1 percent of the peak value divided by the 10-nm bandwidth. The 10-nm bandwidth for the 317.5-nm filter is between the wavelength of 312 and 322 nm, and for the 360-nm filter between 357 and 367 nm. The value of $\overline{T}_\lambda$ for the 317.5-nm filter is 18.6×10^{-6} and for the 360-nm filter 9.34×10^{-6}.

Photometer

Preflight sensitivity measurements (S_λ) for converting photometer counts/pixel per unit transmission to kRa/Å as a function of wavelength for photometers A and B are presented in figure 7. The preflight data were furnished by the University of Iowa and the equipment and procedure used to perform the measurements are described in reference 2.

A preflight calibration was only accomplished for the 360-nm optical-filter photometer system, because preflight measurements of S_λ were limited to wavelengths greater than 317.5 nm. The 360-nm SOI optical filter was mounted in photometer A and the value of $\overline{S}_2$ as obtained from figure 7 averaged over the bandwidth of the 360-nm filter is 12.0 counts/kRa-pixel $\overline{T}_\lambda$. The kilorayleigh (kRa), which is the unit of energy in the definition of S_λ in figure 7, is a unit commonly used for photometric measurements of the airglow and aurora (ref. 10). The constant for converting the 360-nm preflight calibration data from units of kRa/Å to watts/cm^2-cm-sr is 228.7 (kRa/Å)/(watt/cm^2-cm-sr). The derivation of this calibration constant is the subject of appendix A. The calibration of the 317.5-nm optical-filter photometer system, which is the main subject of this report, was obtained from an in-flight technique that is described in subsequent sections.

Conversion of Photometer Counts to Albedos

To obtain R and subsequently Ω from the SOI-measured value of I_λ, it is necessary to use modified data from tables in references 11 and 12 of calculated radiation emerging from a planetary atmosphere with Rayleigh scattering. The data in the reference tables are for a specific wavelength in the form of an atmospheric albedo where the illumination that produced the albedo is from unidirectional solar radiation of π units per unit area normal to the incident direction ($a_{\lambda,c}$). In order to compare I_λ with the modified data, I_λ must be converted to a_λ by multiplying an average value of I_λ ($\overline{I}_\lambda$) having the units of watts/cm^2-cm-sr by π and then dividing it by the average solar flux available over the bandwidth of the optical filter ($\overline{F}_\lambda$). Thus, to compare SOI radiance data with calculated data, equation (6) is modified as follows:

$$a_\lambda = \frac{\pi \overline{I}_\lambda}{\overline{F}_\lambda} \tag{10}$$

However, before $\overline{I}_\lambda$ can be used to obtain a_λ, it must be converted from photometer counts/pixel (C_λ) to watts/cm^2-cm-sr as follows:

$$\overline{I}_\lambda = \frac{C_\lambda}{W_\lambda} \tag{11}$$

where the calibration constant W_λ is

$$W_\lambda = \overline{T}_\lambda \overline{S}_\lambda (\text{Constant})$$

The constant in this equation is the constant for converting the preflight calibration data from kRa/Å to watts/cm^2-cm-sr multiplied by the bandwidth.

The calibration constant for the 360-nm optical-filter photometer system is determined as follows:

$$W_2 \overline{T}_2 \overline{S}_2 \left(228.7 \frac{\text{kRa/Å}}{\text{watt/cm}^2\text{-cm-sr}}\right) (10^2 \text{Å})$$

As discussed in the previous section, bandwidth is 10 nm = 100Å and

$$\overline{T}_2 = 9.34 \times 10^{-6}$$
$$\overline{S}_2 = 12 \text{ counts/pixel-kRa}$$

Thus

$$W_2 = (9.34 \times 10^{-6}) \left(12 \frac{\text{counts}}{\text{pixel-kRa}}\right) \left(228.7 \frac{\text{kRa/Å}}{\text{watt/cm}^2\text{-cm-sr}}\right) (10^2 \text{Å}) = 2.56 \frac{\text{counts/pixel}}{\text{watt/cm}^2\text{-cm-sec}}$$

and from equation (11)

$$\overline{I}_2 = \frac{C_2}{W_2} = 0.391 C_2 \tag{12}$$

It then follows from equations (10) and (12) that C_2 (counts/pixel) detected by the 360-nm optical-filter photometer system can be converted to 360-nm atmospheric albedo data as follows:

$$a_2 \frac{0.391\pi C_2}{1101.6} = (1.11 \times 10^{-3}) C_2 \tag{13}$$

where the average solar flux through the 360-nm filter $(\overline{F}_2)$ is 1101.6 watts/cm^2-cm. This value was obtained by integrating the solar irradiance data in reference 13 over the bandwidth of the 360-nm optical filter and then by dividing the resultant number by the bandwidth.

317.5-nm Photometer System

The conversion factor for relating the C_1 (counts/pixel) detected by the 317.5-nm photometer system to albedo data (a_1) was obtained from an in-flight technique that is described and determined in the results and discussion section of this paper.

Calculated Atmospheric Albedos

Reference 11 contains tables of $a_{2,c}$ from a spherical Earth versus θ at various values of θ_0. The data are valid for ϕ and R equal zero. Techniques and data are also provided to calculate $a_{1,co}$ and $a_{2,c}$ versus θ and θ_0 as a function of R, and in reference 12, equations are available for calculating $a_{1,co}$ and $a_{2,c}$ as a function of ϕ. Let dA in figure 1 represent the area of the SOI-viewed pixel; then θ_0 is the solar zenith angle at the pixel, θ is the SOI view angle at the pixel, and ϕ is the angle between two planes that pass through the center of the Earth, one plane containing the Sun and the observation pixel and the other one containing θ.

Atmospheric Albedos at 360 nm

Figure 8 shows $a_{2,c}$ plotted versus θ for R between 0 and 1.0 at θ_0 of 0°, 30°, 60°, and 75°. The values in figure 8 are in the Sun's vertical plane, a vertical plane passing through the Sun, the center of the Earth, and the spacecraft, and at $\theta_0 = 0°$ they are identical at the same θ for all values of ϕ (see fig. 8(a)). At other values of θ_0 (figs. 8(b), 8(c), and 8(d)), $a_{2,c}$ is not symmetrical about nadir ($\theta = 0°$). The albedo on the solar side (forward scattering side, $\phi = 0°$ to ±90°) is lower at the same θ and R than on the antisolar side (backscattering side, $\phi = \pm 90°$ to 180°). In figures 9, 10, and 11, $a_{2,c}$ is plotted versus ϕ at θ of 30°, 45°, and 60°, respectively, for R between 0 and 1.0 at θ_0 of 20°, 40°, 60°, and 75°. As was the case in figure 8, $a_{2,c}$ on the solar side is lower at the same values of R and θ than it is on the antisolar side.

By interpolation of the data presented in figures 8 to 11, R can be determined by assuming that a_2 equals $a_{2,c}$ for known values of θ_0, θ, and ϕ. Appendix B contains an example of how R is determined from figures 8 to 11.

Ozone-Free Atmospheric Albedos at 317.5 nm

In figure 12, $a_{1,co}$ is plotted for the Sun's vertical plane versus θ for R between 0 and 1.0 at θ_0 of 0°, 30°, 60°, and 75°. In figures 13, 14, and 15, $a_{1,co}$ is plotted versus ϕ at θ of 30°, 45°, and 60°, respectively, for R between 0 and 1.0 at θ_0 of 20°, 40°, 60°, and 75°.

The variation of $a_{1,co}$ in figures 12 to 15 for given values of θ_0, θ, ϕ, and R is similar to the variation of $a_{2,c}$ in figures 8 to 11. At corresponding values of θ_0, θ, and R, $a_{1,co}$ is greater than $a_{2,c}$. When θ and θ_0 are both less than 60° for $R = 0$, the magnitude of the albedo difference is consistent with the concept that the variation in Rayleigh backscattering is inversely proportional to the fourth power of the wavelength. The magnitude of $a_{2,c}$ approaches the magnitude of $a_{1,co}$ with increasing R, and at $R = 1.0$ they are nearly the same. This is illustrated by comparing $a_{2,c}$ in figure 8 with $a_{1,co}$ in figure 12 at the same value of θ.

With a value of R from figures 8 to 11, for a specific combination of θ_0, θ, and ϕ, a value of $a_{1,co}$ can be obtained by linear interpolation of data presented in figures 12 to 15. Appendix B contains an example of how $a_{1,co}$ is determined from figures 12 to 15.

Total Columnar Ozone Measurement

The algorithm defined in equation (9) is used to determine Ω from a value of a_1 obtained from the SOI measurement of I_1. For the algorithm, $a_{1,co}$ is calculated for known values of θ_0, θ, ϕ, and R, where R is first determined from calculated data and the SOI measurement of I_2. The ozone absorption coefficient (α) used in the algorithm is 0.82 (atm-cm)$^{-1}$. ST Systems Corporation (STX), the NASA contractor who developed the computer programs for determining Ω from SOI radiance data, chose 0.82 (atm-cm)$^{-1}$ for α because the National Bureau of Standards experimentally obtained this value at the average ambient temperature of the stratospheric ozone peak (unpublished data). The average relative slant path (s) in the algorithm is the change in attenuation length per unit vertical depth of the absorbing medium with changes in the values of θ_0 and θ. Since the attenuation length in the atmosphere is also a function of Ω, values of s for solving equation (9) have been determined from theoretical calculations for various combinations of θ_0, θ, and ϕ at an average ozone concentration Ω of 300 D.U. and $R = 0.10$. These values are plotted in figure 16 versus $\sec\theta_0 + \sec\theta$ for ϕ of 0°, 90°, and 180°. The quadratic equation

$$s = -0.0613y^2 + 1.181y - 0.133 \qquad (14)$$

where $y = \sec\theta_0 + \sec\theta$ was fitted to the values of s versus y and is represented by the solid line in figure 16. The goodness of the fit of the solid line indicates that the quadratic equation can be used to determine s for all ϕ over the range of y shown.

Results and Discussion

DE-1 Orbit and Ground Track

In table 1 are listed the orbital characteristics of DE-1 on October 22, 1981, and August 17, 1984. The table shows that the major characteristics of the highly elliptical, nearly polar orbit of DE-1 have changed very little during the first 3 years of the satellite's lifetime. The orbital period of DE-1, 6 hours and 50 minutes, results in approximately 3.5 orbits of the Earth each day. The Earth tracks of the sunlit portions of these orbits on October 1 and 2, 1981, are shown in figure 17. On October 1, the first track was over western Asia, the second over the South and North Atlantic Oceans, the third over the eastern portion of the Pacific Ocean, and a portion of a fourth track over Australia. On October 2, the track begins over eastern Asia and follows in sequence over Africa and Europe, South and North America, and the western Pacific Ocean. On October 3, the October 1 tracks were repeated with each track processed to the west by approximately 1°. The open circles along the South and North America track on October 2 indicate the location of the center of the scenes obtained with SOI during that pass. Because the perigee of the DE-1 orbit was located over the Earth's South Pole on October 2, the high satellite velocity and the 12-minute interval required to obtain an SOI scene limited the number of scenes that could be taken over South America; but these scenes have the best possible spatial resolution (Pixel size $\geq$ 3 km). However, over North America where apogee was located (Pixel size $\approx$ 120 km), the low satellite velocity allowed many overlapping scenes to be recorded. Since the perigee of the DE-1 orbit precesses at approximately 0.33°/day or approximately 10°/month, the available scenes in the Northern Hemisphere diminished with time while those in the Southern Hemisphere increased. In October 1984, the first perigee cycle was completed and the SOI instrument continued to operate properly.

SOI Data

The areas encompassed by the solid lines in figure 17 show the extent of SOI scenes that were recorded during the North Atlantic and eastern Pacific passes on October 1, 1981. The shapes of the two scenes are not identical because they were taken from different altitudes in the orbit. The North Atlantic scene reaches from western United States to eastern Europe and overlaps the center of two adjacent ground tracks on October 2, 1981. The eastern Pacific scene also overlaps the centers of two October 2 ground tracks, as well as a portion of the North Atlantic scene over North America on the same day. Since 15 scenes that included North America were recorded on the North Atlantic and eastern Pacific passes on October 1, and 15 scenes on the North America pass on October 2, three 2.5-hour continuous Ω mapping periods were recorded over North America on those 2 days. Figure 18 shows an Ω contour map generated from a 15th order–15th degree spherical harmonic model of the SOI Ω data obtained on October 1, 1981, during the eastern Pacific pass from the scene area outlined in figure 17. The high-Ω areas are designated by H (380 D.U.) and the low concentration areas by L (250 D.U.). Contour maps showing more detail can also be generated from the SOI Ω data by averaging the data in small latitude-longitude blocks. Thus, it is seen in figures 17 and 18 that Ω can be mapped daily over large areas of the Earth's surface for hours at a time. From September 23, 1981, to June 14, 1984, Ω data have been recorded from SOI on 470 days during one or more

of the DE-1 daily orbits. All these days are listed in table 2.

Validation of Reflectivity

Presented in table 3 are required SOI data for determining R from C_2 between the Earth longitudes of 99.5°W and 71.9°W along 25°N latitude on October 2, 1981, at 1716 universal time (UT). This data set was chosen because the GOES cloud picture taken at 1500 UT on October 2, 1981, shows that at 25°N latitude, light sporadic clouds existed over the Gulf of Mexico and light and heavy clouds existed over the western Atlantic Ocean, thus assuring that a large variation in reflectivity over water would be included in the data set. The presence of clouds causes the large variation in C_2 seen in table 3, where C_2 varies from 150 to 250 counts/pixel over areas containing light sporadic clouds, and to over 600 counts/pixel from areas containing heavy clouds. Using equation (13), C_2 was converted to a_2 and then tabulated in table 3. The conversion was made in order to determine R for each data point location in table 3 from the data in figures 8 to 11 after assuming that a_2 equals $a_{2,c}$ at the specific values of θ_0, θ, and ϕ at each location. The calculated values of R are listed in table 3 and plotted in figure 19 versus the longitude location of each data point.

In figure 19, R varies from a minimum value of 0.03 over land (longitude 98.8°W) to between 0.09 to 0.23 over the Gulf of Mexico where light sporadic clouds are visible in the GOES scene at 1500 UT on the same day and to a value of 0.85 over the Atlantic Ocean where heavy clouds existed. The minimum value of R over the Gulf of Mexico ranging from 0.09 to 0.10 in figure 19 is within the accuracy range of a value of R over open ocean determined in reference 9 at the wavelength of 360 nm. In that report, a measurement of $R = 0.1055 \pm 0.0089$ was made from an altitude of 1000 ft for $\theta_0 = 27°$, and a linear extrapolation of this measurement in conjunction with other higher altitude measurements resulted in an ocean level value of $R = 0.918$. Thus, it is evident from the comparison of the minimum value of R determined from SOI radiance data over the Gulf of Mexico with the value of R over open ocean published in reference 9, that the preflight calibration and the theoretical conversion data are satisfactory for determining R from the SOI measurement of C_2.

In-Flight Calibration of 317.5-nm Photometer System

An in-flight calibration to determine the conversion factor for converting C_1 with the units of counts/pixel to a_1 was performed using Dobson ground station Ω measurements as the calibration reference. This was accomplished by calculating a_1 from equation (9), after substituting into the equation the value of Ω measured at Dobson stations along with the appropriate values of s and $a_{1,co}$. The conversion factor was then determined by averaging the ratio of a_1 to C_1 obtained from all the Dobson station locations.

Dobson station Ω data. Presented in table 4 are Ω data measured by Canadian and United States Dobson stations for September 29 and October 1 to 3, 1981. The total ozone (Ω) is expressed in the Dobson unit, which is defined as 10^{-3} centimeter of ozone at 0°C and at standard sea-level pressure. The Canadian network data were obtained from the Dobson working group at the World Ozone Data Center, Atmospheric Environment Service, Department of Environment, Downsview, Ontario, Canada (WODC), and the United States network data from the NOAA Environmental Research Laboratories, Boulder, Colorado. The data in table 4 for each station consist of single or multiple daily measurements with only one of the measurements eventually published in *Ozone Data for the World* by WODC (ref. 14). The data published by WODC are identified in the table.

The first number under the heading "Conditions" in table 4 refers to the wavelengths at which the data were obtained with the Dobson spectrometer as described in reference 14, and the second number refers to the kind of observation.

The Dobson station locations shown in table 4 were viewed by the SOI system on DE-1 one or more times during the days listed, thus, providing 33 or more ground station Ω data samples for the in-flight calibration at 317.5 nm.

317.5-nm photometer calibration. In table 5 are listed average values of θ_0, θ, and ϕ $\left(\overline{\theta}_0, \overline{\theta}, \text{ and } \overline{\phi}\right)$ from five, consecutive, 12-minute SOI scenes at the location of the Dobson stations named in table 4 on September 29 and October 1 to 3, 1981. The times shown during each of the DE-1 orbital passes are the mean times of the five consecutive scenes. Also shown in table 5 are average values of C_1 and C_2 ($\overline{C}_1$ and $\overline{C}_2$) resulting from dividing the total SOI counts from each photometer during 1 hour from all pixels in a 6° latitude by 6° longitude block centered at the location of the Dobson stations by the total number of pixels. The total number of pixels for each station as listed in table 5 show that for 85 percent of the stations, the number of pixels used to determine $\overline{C}_1$ and $\overline{C}_2$ exceeded 100. Thus, for those station locations, the number of counts used to obtain $\overline{C}_1$

and $\overline{C}_2$ exceeded the value of $\overline{C}_1$ and $\overline{C}_2$ by at least a factor of 100.

In table 5, the value of a_2 converted from $\overline{C}_2$ is tabulated, and from a_2, $\overline{\theta}_0$, $\overline{\theta}$, and $\overline{\phi}$ in table 5, R was obtained for each Dobson station location by interpolation of the data contained in figures 8 to 11. With the value of R, it is possible to obtain $a_{1,co}$ from figures 12 to 15. Then from $a_{1,co}$, $\overline{s}$ (from table 6), and an ozone absorption coefficient of 0.82 $(\text{atm-cm})^{-1}$, the values of a_1 were calculated $(a_{1,c})$ using equation (9) after substituting into the equation the Dobson station Ω value from the SOI observation and Dobson station closest measurement times listed in tables 4 and 5. Values of $a_{1,c}$ calculated in this manner for each Dobson station observation and SOI overflight on September 29 and October 1 to 3, 1981, are tabulated in table 6 and plotted in figure 20 versus $\overline{C}_1$ listed in table 5 for each station location.

The solid line in figure 20 with its intercept at 0 has a slope of 0.001. Since, with the exception of some data obtained during intermittent rain conditions (solid symbols), the data are concentrated on both sides and along the constant ratio line, it is seen that the response of the DE-1 photometer is essentially linear with an increasing albedo. Therefore, a linear regression or even an arithmetic average of $a_{1,c}/\overline{C}_1$ data for non-rain conditions seems suitable for determining the SOI 317.5-nm conversion factor. However, it is seen in figure 21, where $a_{1,c}/\overline{C}_1$ for non-rain conditions from the various orbital passes is plotted against $\overline{\theta}_0$, that the scatter in the calculated SOI 317.5-nm conversion factor becomes higher at $\overline{\theta}_0 > 70°$. When $\overline{C}_1$ in table 5 is multiplied by the number of pixels used to obtain $\overline{C}_1$ at $\overline{\theta}_0 > 70°$, the number of counts varied from 50 to 7500, well below the average counts of 18 450 from all the data in table 5. Thus, because of insufficient counts, all calibration data at $\overline{\theta}_0 > 70°$ were excluded from the data that were used for determining the 317.5-nm conversion factor.

Another second order effect on the SOI 317.5-nm conversion factor is seen in figure 22, where $a_{1,c}/\overline{C}_1$ obtained from 51 data points where non-rain conditions existed at $\overline{\theta}_0 \leq 70°$ is plotted against SOI scan line number (N) from table 6. The SOI nadir scan line is designated as scan line number 62 with the left portion of a scene diminishing and the right portion increasing in number from the nadir scan line. A linear regression analysis of the data indicates with a correlation coefficient of -0.50 that there is a linear reduction in the SOI 317.5-nm conversion factor (K) with increasing scan line number (solid line). The two-sigma variations of ± 50 percent in the regression coefficient and ± 2.6 percent in the zero scan line value are indicated by the dashed lines in figure 22. The dashed lines also show the left to right reduction in K. The linear reduction, seen in figure 22 as the solid line, calculated from the equation

$$K = -(0.6421 \times 10^{-6})N + (1.0631 \times 10^{-3}) \quad (15)$$

would result in a maximum bias of 6 percent in the determination of SOI total ozone between extremities of an SOI 317.5-nm radiance scene, if the SOI conversion factor is not normalized to the nadir viewing location by the use of K.

Comparison Between SOI and Dobson Station Total Ozone

The SOI total ozone values Ω were calculated as follows from 51 SOI data recordings at Dobson station locations where non-rain conditions and $\overline{\theta}_0 \leq 70°$ existed on September 29 and October 1 to 3, 1981. First, values of $\overline{C}_1$ in table 5 were converted to a_1 by multiplying them by K. The conversion factor K was determined from N in table 6 using linear equation (15). These values of a_1, along with appropriate values of $\overline{s}$ and $a_{1,co}$ from table 6 and an ozone absorption coefficient α of 0.82 $(\text{atm-cm})^{-1}$, were substituted in equation (9) to obtain Ω. The 51 values of Ω calculated in this manner are plotted in figure 23 versus the Dobson station values of Ω. Clear, medium, and heavy cloud conditions existing at the ground stations are identified by the various symbols. On some days more than one Dobson station value of Ω or more than one SOI Dobson station sighting was obtained. The closest daily times are identified in figure 23 by the solid symbols. The solid line in the figure is the perfect data correlation line having its intercept pass through zero and a slope equal to 1. The standard deviation of the 51 total ozone determinations from the perfect data correlation line was calculated to be 3.4 percent, and when only the closest daily times are considered, the standard deviation improved to 2.4 percent. A part of this scatter is due to the different measurement precision of individual Dobson stations. Thus, the precision of the SOI Ω data is estimated to be better than 2.4 percent. The accuracy of a Ω measurement from SOI depends on the accuracy of the Ω measured by the Dobson ground stations, because the SOI total system calibration depends on ground station Ω data. It is estimated in reference 15 that there is a possible systematic error of about 5 percent associated with Dobson spectrophotometer observations.

Tabulated in figure 23 are the calculated linear regression correlation coefficients between Dobson station and SOI total ozone determinations for clear, medium, and heavy ground station cloud conditions. The coefficients are listed from the analysis based on

all SOI and Dobson station recording times and then again for only the closest daily times. The coefficients show that the SOI algorithm for the determination of total ozone is as effective for heavy cloud conditions as it is on clear days; if anything, it improves with increasing cloud conditions because the coefficients increase with increasing cloud conditions. Considering only closest daily times, the average correlation coefficient is 0.959.

Conclusions

This paper presents the calibrations, outlines the measurement technique, and provides theoretical backscattered radiance values for determining scene reflectivity and total columnar ozone from the Spin-Scan Ozone Imager (SOI), a part of the auroral imaging instrumentation aboard the Dynamics Explorer 1 Satellite (DE-1).

From comparison of cloud scenes generated from DE-1 radiance data with cloud scenes from the Geostationary Operational Environmental Satellite (GOES), it is evident that the pixel location system of DE-1 is not a limiting factor for producing total ozone maps to a spatial accuracy of $\pm 1°$.

Calculated linear regression analysis correlation coefficients between total ozone determinations from Dobson stations and from SOI indicate that the SOI total ozone determination is as effective for cloud conditions as it is on clear days with an average correlation coefficient for clear and cloudy conditions of 0.959. The precision of the SOI ozone data is estimated to be better than 2.4 percent.

NASA Langley Research Center
Hampton, VA 23665-5225
June 1, 1987

Appendix A

Relation Between Photometric Units

The kilorayleigh (kRA) is the unit of energy in the definition of S in figure 7 and is a unit commonly used for photometric measurements of the airglow and aurora. As discussed in reference 10, kilorayleighs are reported in terms of $4\pi B$, rather than the surface brightness B itself. In reference 10, B is in units of 10^6 photons/cm^2-sec-sr. However, 1Ra = 10^6 photons/cm^2-sec because Ra multiplied by 4π is just the measured brightness.

Since photons have different energies at different wavelengths, for the SOI experiment, average energy over the bandwidth of the photometer system must be calculated to convert photometer-measured radiation energies in kRa/Å to watts/cm^2-cm-sr, units common to backscattered scene spectral radiance (I_λ). The calculations can be performed as follows:

$$E = h\frac{c}{\lambda} \tag{A1}$$

where E is the energy in joules/photon, c is the velocity of light (3×10^8 m/sec), λ is the wavelength in meters, and h is Planck's constant (6.63×10^{-34} joule-sec). The average value of E calculated for the 360-nm optical-filter photometer system over the bandwidth of the filter using equation (A1) is 5.495×10^{-19} joule/photon. Since 1 joule/sec = 1 watt and 4πRa = 10^6 photons/cm^2-sec-sr, then the constant for converting the 360-nm photometer system preflight calibration data from the units of kRa/Å to watts/cm^2-cm-sr can be determined as follows:

$$\begin{aligned} 1\frac{\text{watt}}{\text{cm}^2\text{-cm-sr}} &= 1\ \frac{\text{joule/sec}}{\text{cm}^2\text{-cm-sr}}\left(10^{-8}\frac{\text{cm}}{\text{Å}}\right)\left(\frac{1}{5.495 \times 10^{-19}\ \text{joule/photon}}\right)\left(\frac{4\pi\text{kRa}}{10^3 10^6\ \text{photons/cm}^2\text{-sec-sr}}\right) \\ &= \frac{4\pi}{5.495 \times 10^{-2}}\text{kRa/Å} = 228.7\ \text{kRa/Å} \end{aligned} \tag{A2}$$

Appendix B

Determination of SOI Scene Reflectivity and 317.5-nm Atmospheric Albedos in the Absence of Ozone

From the 360-nm SOI measurement of albedo (a_2) and the values of solar zenith angle (θ_0), view angle (θ), and azimuth angle (ϕ) from an SOI scene location, it is possible to determine scene reflectivity (R) using the calculated information presented in figures 8 to 11. For example, from the SOI measured value of a_2 of 0.161π per unit area at $\overline{\theta}_0 = 69.6°$, $\overline{\theta} = 37.1°$, and $\overline{\phi} = 84.8°$, respectively, R is determined to be 0.30 for the Bismarck Dobson station location on September 29, 1981, at 1443 UT (tables 5 and 6). The procedure for determining R from the figures is as follows: At $\phi = 84.8°$ and $a_2 = 0.161$ in figures 9(c) and 9(d), $R = 0.12$ and 0.40, respectively. Linear interpolation of R at $\theta = 30°$ between $\theta_0 = 60°$ and 75° results in $R = 0.30$ at $\theta_0 = 69.6°$. At $\phi = 84.8°$ and $a_2 = 0.161$ in figures 10(c) and 10(d), $R = 0.11$ and 0.39, respectively. Linear interpolation of R at $\theta = 45°$ between $\theta_0 = 60°$ and 75° results in $R = 0.29$ at $\theta_0 = 69.6°$. Finally, a third linear interpolation between $\theta = 30°$ and 45° results in $R = 0.30$ at $\phi = 84.8°$, $\theta_0 = 69.6°$, and $\theta = 37.1°$ when $a_2 = 0.161\pi$ per unit area.

The 317.5-nm albedo radiance in the absence of ozone ($a_{1,co}$) is determined using R and the calculated information presented in figures 12 to 15. The procedure for determining $a_{1,co}$ from the figures is as follows: At $\phi = 84.8°$ and $R = 0.30$ in figures 13(c) and 13(d), $a_{1,co} = 0.24$ and 0.11, respectively. Linear interpolation of $a_{1,co}$ at $\theta = 30°$ between $\theta_0 = 60°$ and 75° results in $a_{1,co} = 0.157$ at $\theta_0 = 69.6°$. At $\phi = 84.8°$ and $R = 0.30$ in figures 14(c) and 14(d), $a_{1,co} = 0.27$ and 0.14, respectively. Linear interpolation of $a_{1,co}$ at $\theta = 45°$ between $\theta_0 = 60°$ and 75° results in $a_{1,co} = 0.187$ at $\theta_0 = 69.6°$. Finally, a third linear interpolation between $\theta = 30°$ and 45° results in $a_{1,co} = 0.170$ at $\phi = 84.8°$, $\theta_0 = 69.6°$, and $\theta = 37.1°$ when $R = 0.30$.

References

1. Keating, G. M.; Craven, J. D.; Frank, L. A.; Young, D. F.; and Bhartia, P. K.: Initial Results From the DE-1 Ozone Imaging Instrumentation. *Geophys. Res. Lett.*, vol. 12, no. 9, Sept. 1985, pp. 593–596.
2. Frank, L. A.; Craven, J. D.; Ackerson, K. L.; English, M. R.; Eather, R. H.; and Carovillano, R. L.: Global Auroral Imaging Instrumentation for the Dynamics Explorer Mission. *Space Sci. Instrum.*, vol. 5, no. 4, Dec. 1981, pp. 369–393.
3. Dave, J. V.; and Mateer, Carlton L.: A Preliminary Study on the Possibility of Estimating Total Atmospheric Ozone From Satellite Measurements. *J. Atmos. Sci.*, vol. 24, no. 4, July 1967, pp. 414–427.
4. Mateer, Carlton L.; Heath, Donald F.; and Krueger, Arlin J.: Estimation of Total Ozone From Satellite Measurements of Backscattered Ultraviolet Earth Radiance. *J. Atmos. Sci.*, vol. 28, no. 7, Oct. 1971, pp. 1307–1311.
5. Klenk, K. F.; Bhartia, P. K.; Fleig, A. J.; Kaveeshwar, V. G.; McPeters, R. D.; and Smith, P. M.: Total Ozone Determination From the Backscatter Ultraviolet (BUV) Experiment. *J. Appl. Meteorol.*, vol. 21, no. 11, Nov. 1982, pp. 1672–1684.
6. Fleig, A. J.; Klenk, K. F.; Bhartia, P. K.; and Gordon, D.: *User's Guide for the Total-Ozone Mapping Spectrometer (TOMS) Instrument First-Year Ozone-T Data Set.* NASA RP-1096, 1982.
7. Dave, J. V.: Meaning of Successive Iteration of the Auxiliary Equation in the Theory of Radiative Transfer. *Astrophys. J.*, vol. 140, 1964, pp. 1292–1303.
8. Craig, Richard A.: *The Upper Atmosphere—Meteorology and Physics.* Academic Press, Inc., c.1965.
9. Doda, D. D.; and Green, A. E. S.: Surface Reflectance Measurements in the UV From an Airborne Platform, Part I. *Appl. Opt.*, vol. 19, no. 13, July 1, 1980, pp. 2140–2145.
10. Hunten, D. M.; Roach, F. E.; and Chamberlain, J. W.: A Photometric Unit for the Airglow and Aurora. *J. Atmos. & Terr. Phys.*, vol. 8, no. 6, June 1956, pp. 345–346.
11. Dave, J. V.; and Furukawa, P. M.: Scattered Radiation in the Ozone Absorption Bands at Selected Levels of a Terrestrial, Rayleigh Atmosphere. *Meteorol. Monogr.*, vol. 7, no. 29, Jan. 1966.
12. Coulson, Kinsell L.; Dave, Jitendra V.; and Sekera, Zdenek: *Tables Related to Radiation Emerging From a Planetary Atmosphere With Rayleigh Scattering.* University of California Press, 1960.
13. *Solar Electromagnetic Radiation—NASA Space Vehicle Design Criteria.* NASA SP-8005, 1965.
14. *Ozone Data for the World—Catalogue of Ozone Stations and Catalogue of Ozone Data for 1981.* Index No. 16, Atmospheric Environment Service, Dep. of Environment (Downsview, Ontario).
15. Komhyr, W. D.: Dobson Spectrophotometer Systematic Total Ozone Measurement Error. *Geophys. Res. Lett.*, vol. 7, no. 2, Feb. 1980, pp. 161–163.

Table 1. Dynamics Explorer 1 (1981 070A, DE-1) Orbital Characteristics

	October 22, 1981	August 17, 1984
Semimajor axis, km	18 305	18 296
Eccentricity	0.6219	0.6210
Inclination, deg	89.90	89.63
Motion of perigee, deg/day	−0.3308	−0.3301
Anomalistic period, min	410.77	410.49
Height of perigee, km	543.38	556.42
Height of apogee, km	23 309.64	23 279.58
Velocity at perigee, km/hr	34 792	34 750
Velocity at apogee, km/hr	8112	8125

Table 2. Days When SOI Recorded Total Ozone Data up to June 14, 1984

Year	Days
1981	266 to 278, 280 to 336, 338 to 351, 353 to 356, and 358 to 365
1982	1 to 5, 7 to 10, 13, 15 to 35, 81 to 86, 88 to 94, 96 to 140, 142, 144, 208, 210 to 220, 274, 276, and 309 to 315
1983	9, 11, 13, 15 to 40, 81 to 147, 168, 170, 177, 179, 181, 183, 185, 187, 203, 205, 208 to 211, 322, 324, 326, 328, 330, 332, 334, 336, 338, 340, 342, 344, 346, 348, 350 to 360, 362, and 364
1984	1 to 4, 6 to 17, 19, 21, 23, 25, 27, 29, 31, 33 to 40, 82, and 84 to 166

Table 3. SOI Data for Determining Reflectivity Along 25°N Latitude on October 2, 1981, at 1716 UT

Latitude, deg N	Longitude, deg W	θ_0, deg	θ, deg	ϕ, deg	C_2, counts/pixel	a_2, π units/unit area (a)	R (b)
25.0	99.5	36.7	25.2	32.6	152	0.169	0.06
24.8	98.8	36.2	25.5	30.3	144	.160	.03
24.8	98.1	35.8	25.6	27.8	200	.222	.15
24.7	97.4	35.4	25.8	25.4	176	.195	.10
24.6	96.7	34.9	26.2	23.2	184	.204	.12
25.1	96.0	34.9	25.6	19.7	184	.204	.12
25.9	95.3	34.5	25.8	17.2	168	.187	.11
24.8	94.6	34.0	26.4	15.2	200	.222	.13
24.7	93.9	33.5	26.7	12.9	200	.222	.13
24.6	93.2	33.1	27.2	10.7	200	.222	.13
25.1	92.5	33.1	26.8	7.1	200	.222	.13
25.0	91.8	32.7	27.3	4.9	184	.204	.12
24.8	91.1	32.3	27.8	2.8	224	.249	.20
24.7	90.3	31.9	28.3	.6	224	.249	.20
24.6	89.6	31.5	28.8	1.6	208	.231	.13
25.1	88.9	31.6	28.6	5.2	184	.204	.10
24.9	88.2	31.2	29.2	7.2	192	.213	.12
24.7	87.5	30.7	29.9	9.1	248	.275	.23
24.6	86.8	30.4	30.4	11.3	200	.222	.11
24.9	86.0	30.4	30.5	14.5	216	.240	.16
24.7	85.3	30.1	31.2	16.5	224	.249	.18
24.5	84.6	29.7	31.9	18.4	240	.266	.21
25.0	83.8	29.9	31.9	22.0	192	.213	.10
24.8	83.1	29.5	32.6	23.9	184	.204	.09
24.7	82.3	29.2	33.3	25.9	216	.240	.15
25.0	81.5	29.4	33.6	29.0	176	.195	.08
25.3	80.7	29.5	33.9	32.0	192	.213	.10
25.1	80.0	29.1	34.7	33.9	200	.222	.11
24.8	79.3	28.8	35.5	35.7	208	.231	.13
24.6	78.5	28.5	36.3	37.5	216	.240	.16
25.0	77.7	28.8	36.6	40.8	272	.302	.28
25.2	76.9	29.0	37.0	43.6	336	.373	.41
25.0	76.1	28.7	37.9	45.4	368	.409	.40
24.7	75.3	28.4	38.8	47.2	352	.391	.44
25.0	74.4	28.7	39.3	50.1	576	.639	.76
25.4	73.5	29.1	39.7	53.1	608	.675	.80
25.0	72.7	28.8	40.7	54.9	640	.702	.85
24.7	71.9	28.5	41.7	56.5	640	.702	.84

[a] Converted from C_2 using preflight calibration data (eq. (13)).
[b] Calculated reflectivity from SOI data at 360 nm.

Table 4. Dobson Ground Station Total Ozone Data

Station	Conditions (a)	Universal time	Ozone D.U.
September 29, 1981			
Bismarck—47°N–101°W	0–4	1624	[b]292
	0–4	1832	282
Boulder—40°N–105°W	0–4	1629	277
	0–4	1931	[b]278
Caribou—47°N–60°W	0–5	1527	[b]351
	0–5	1701	347
	0–5	1847	353
	0–5	1906	360
Churchill—59°N–94°W	0–2	1525	[b]325
Edmonton—54°N–108°W	3–4	1652	340
	3–4	1720	348
	0–4	1722	349
	0–4	1923	[b]352
Goose Bay—53°N–60°W	[c]3–6	1206	320
	[c]3–6	1252	316
	[c]0–6	1506	341
	[c]0–6	1550	[b]357
Toronto—44°N–79°W	0–4	1659	[b]317
Wallops Island—38°N–76°W	0–0	1500	304
	0–0	1700	[b]304
	0–0	1900	308
White Sands—32°N–106°W	0–0	1700	[b]276
October 1, 1981			
Bismarck	0–2	1900	[b]292
Boulder	0–0	1600	[b]277
Caribou	0–6	1500	[b]318
Churchill	3–4	1816	[b]338
Edmonton	3–5	1549	292
	3–5	1727	312
	0–5	1920	[b]309
Goose Bay	3–5	1209	324
	3–5	1253	330
	0–5	1340	322
	0–5	1554	[b]323
Toronto	0–6	1734	[b]346
Wallops Island	0–0	1900	[b]297
White Sands	0–5	1700	[b]279

[a]The first number refers to which wavelengths were used to record the ozone data, and the second number to the kind of observation defined as follows:

0—on direct Sun
1—on direct Moon
2—on blue zenith sky
3—on zenith clouds (uniform stratified layer of small opacity)
4—on zenith clouds (uniform or moderate variable layer of medium opacity)
5—on zenith clouds (uniform or moderately variable layer of large opacity)
6—on zenith clouds (highly variable opacity, with or without precipitation stations reporting rain or snow occurring)

[b]Value also published in *Ozone Data for the World* (ref. 14).
[c]Dobson station reported rain.

Table 4. Concluded

Station	Conditions (a)	Universal time	Ozone D.U.
October 2, 1981			
Bismarck	0–0	1705	296
	0–0	1932	282
Boulder	0–4	2100	[b]273
Churchill	0–4	1807	[b]310
Edmonton	3–4	1558	318
	3–3	1740	331
	0–3	1742	330
	0–3	1850	[b]337
Goose Bay	3–5	1212	323
	[c]0–6	1358	[b]331
Nashville—36°N–87°W	0–0	1600	317
Toronto	0–5	1545	[b]355
Wallops Island	[c]0–6	1500	[b]333
	[c]0–6	1602	344
	[c]0–6	1700	367
	[c]0–6	1900	364
White Sands	0–6	1900	285
October 3, 1981			
Churchill	0–4	1806	[b]307
Edmonton	3–2	1600	339
	3–3	1739	345
	0–3	1741	347
	0–4	2020	[b]347
Goose Bay	[c]0–6	1555	[b]326
Nashville	0–0	1800	309
Wallops Island	0–5	1900	[b]339
White Sands	0–6	1900	285

[a]The first number refers to which wavelengths were used to record the ozone data, and the second number to the kind of observation defined as follows:

0—on direct Sun
1—on direct Moon
2—on blue zenith sky
3—on zenith clouds (uniform stratified layer of small opacity)
4—on zenith clouds (uniform or moderate variable layer of medium opacity)
5—on zenith clouds (uniform or moderately variable layer of large opacity)
6—on zenith clouds (highly variable opacity, with or without precipitation stations reporting rain or snow occurring)

[b]Value also published in *Ozone Data for the World* (ref. 14).
[c]Dobson station reported rain.

Table 5. SOI Data for Calibration at 317.5 nm Using Dobson Station Total Ozone Data

Station	[a] $\overline{\theta}_0$, deg	[a] $\overline{\theta}$, deg	[a] $\overline{\phi}$, deg	$\overline{C}_2$, counts/pixel	a_2, π units/unit area (b)	$\overline{C}_1$, counts/pixel	No. of pixels[c]
September 29, 1981, 1443 UT[d]; Atlantic pass							
Bismarck	69.6	37.1	84.8	144.9	0.161	68.1	130
Boulder	70.0	44.6	89.4	154.9	.172	72.5	111
Caribou	53.6	29.9	28.4	317.3	.352	139.8	147
Churchill	72.1	21.8	84.3	132.1	.147	56.2	118
Edmonton	74.0	31.7	82.1	188.4	.209	63.0	58
Goose Bay	57.0	23.4	7.5	392.8	.436	194.2	131
Toronto	56.4	34.1	51.5	274.4	.305	136.6	139
Wallops Island	50.4	39.7	46.9	161.6	.179	107.5	137
White Sands	69.0	53.7	91.1	135.2	.150	66.9	102
September 29, 1981, 2118 UT[d]; Eastern Pacific pass							
Bismarck	60.1	48.6	91.0	269.8	0.300	137.1	117
Boulder	54.0	51.4	85.0	260.1	.289	145.7	118
Churchill	72.0	43.7	104.3	124.3	.138	54.7	94
Edmonton	63.7	39.1	91.1	297.8	.330	121.9	127
Toronto	72.6	60.9	103.7	153.6	.171	62.8	50
White Sands	46.8	56.9	82.3	228.0	.253	143.7	96
September 29, 1981, 2218 UT[d]; Eastern Pacific pass							
Bismarck	69.2	51.7	75.9	206.3	0.229	89.1	83
Boulder	63.7	57.7	73.6	240.8	.267	111.6	78
Churchill	76.0	41.0	88.3	91.6	.102	36.5	20
Edmonton	70.3	41.6	71.3	225.9	.251	81.3	91
Toronto	76.6	61.0	93.8	160.0	.178	50.0	1
White Sands	56.2	62.0	75.5	228.0	.253	128.4	10
October 1, 1981, 1424 UT[d]; Atlantic pass							
Bismarck	72.6	34.3	95.8	142.7	0.158	51.5	126
Boulder	72.7	42.2	95.6	99.3	.110	48.9	108
Caribou	55.9	23.0	38.7	211.0	.234	108.8	162
Churchill	74.2	19.1	99.8	89.3	.099	36.9	108
Edmonton	76.0	28.9	91.2	150.7	.167	50.5	19
Goose Bay	58.6	16.3	10.7	256.5	.285	124.0	150
Toronto	59.9	27.7	66.4	385.1	.428	179.6	168
Wallops Island	53.6	33.9	57.0	287.1	.319	153.0	170
White Sands	71.9	51.4	96.5	203.8	.226	80.3	104

[a] Hourly average for Dobson station location.
[b] Converted from $\overline{C}_2$ using preflight calibration data (eq. (13)).
[c] Number of pixels in a 6° latitude × 6° longitude block centered on the Dobson station location.
[d] Center Universal Time of five SOI 12-minute scenes.

Table 5. Continued

Station	[a] $\overline{\theta}_0$, deg	[a] $\overline{\theta}$, deg	[a] $\overline{\phi}$, deg	$\overline{C}_2$, counts/pixel	a_2, π units/unit area ([b])	$\overline{C}_1$, counts/pixel	No. of pixels[c]
October 1, 1981, 1524 UT[d]; Atlantic pass							
Bismarck	65.2	42.9	60.5	200.5	0.223	89.4	84
Boulder	64.5	50.2	66.3	132.6	.147	78.1	72
Caribou	51.6	43.2	12.7	248.3	.276	128.8	94
Churchill	69.6	28.0	49.3	112.9	.125	53.9	80
Edmonton	72.8	34.3	66.7	193.4	.215	70.7	81
Goose Bay	56.5	37.0	2.8	278.8	.310	132.4	102
Toronto	53.9	43.0	33.6	457.4	.508	219.2	65
Wallops Island	47.0	50.7	29.4	339.7	.377	177.6	81
White Sands	63.0	58.1	72.4	309.1	.343	132.5	49
October 1, 1981, 1951 UT[d]; Eastern Pacific pass							
Bismarck	54.1	55.3	118.7	215.2	0.239	129.4	138
Boulder	48.0	52.5	112.1	175.4	.195	124.8	162
Churchill	67.6	56.1	125.6	185.7	.206	83.8	53
Edmonton	59.8	52.3	125.0	284.7	.316	138.2	136
White Sands	40.7	51.0	95.6	360.9	.400	213.0	103
October 1, 1981, 2051 UT[d]; Eastern Pacific pass							
Bismarck	59.4	49.1	93.7	173.5	0.193	98.6	131
Boulder	52.9	51.0	87.3	155.3	.172	101.7	127
Churchill	71.2	46.0	108.0	130.2	.145	56.1	104
Edmonton	63.4	40.1	96.2	221.6	.246	110.9	134
Toronto	72.6	61.2	104.3	248.3	.272	74.8	26
White Sands	45.6	55.9	83.9	346.1	.384	188.5	101
October 2, 1981, 1628 UT[d]; North America pass							
Bismarck	57.3	27.1	145.9	163.0	0.181	109.0	380
Boulder	55.3	29.6	147.1	233.8	.260	143.3	575
Churchill	64.7	39.3	142.7	211.9	.235	104.5	186
Edmonton	65.5	34.4	157.2	286.1	.318	126.4	226
Goose Bay	75.5	51.6	123.7	309.0	.343	151.2	175
Nashville	44.1	30.3	105.5	194.8	.216	139.5	638
Toronto	49.3	34.1	113.7	394.8	.438	193.7	366
Wallops Island	43.0	34.2	101.4	388.6	.431	213.8	410
White Sands	51.6	27.9	140.8	341.9	.380	195.0	741

[a]Hourly average for Dobson station location.
[b]Converted from $\overline{C}_2$ using preflight calibration data (eq. (13)).
[c]Number of pixels in a 6° latitude × 6° longitude block centered on the Dobson station location.
[d]Center Universal Time of five SOI 12-minute scenes.

Table 5. Concluded

Station	[a] $\overline{\theta}_0$, deg	[a] $\overline{\theta}$, deg	[a] $\overline{\phi}$, deg	$\overline{C}_2$, counts/pixel	a_2, π units/unit area (b)	$\overline{C}_1$, counts/pixel	No. of pixels[c]
October 2, 1981, 1728 UT[d]; North America pass							
Bismarck	53.0	14.7	19.5	119.8	0.133	91.0	226
Boulder	48.9	20.4	16.4	209.1	.232	136.7	233
Churchill	63.1	15.9	87.1	156.0	.173	85.8	165
Edmonton	61.7	8.5	69.8	286.7	.318	139.6	195
Goose Bay	60.7	39.4	91.5	240.0	.263	118.3	145
Nashville	41.0	32.8	29.8	159.3	.177	121.6	206
Toronto	49.1	30.8	58.2	374.7	.415	180.4	196
Wallops Island	43.8	38.4	56.8	368.2	.409	197.7	187
White Sands	43.0	29.8	30.6	343.4	.381	206.1	228
October 2, 1981, 1828 UT[d]; North America pass							
Bismarck	50.9	37.6	11.5	143.4	0.159	101.9	115
Boulder	45.2	43.6	4.4	247.7	.275	154.5	113
Churchill	63.0	25.6	33.6	160.9	.179	85.9	108
Edmonton	59.1	27.1	5.8	299.5	.333	152.5	116
Goose Bay	66.2	42.4	71.1	198.0	.220	87.5	97
Nashville	42.6	51.5	33.0	177.2	.197	123.3	96
Toronto	52.3	44.9	45.9	380.6	.423	165.7	108
Wallops Island	48.6	52.6	51.3	363.6	.405	170.1	98
White Sands	37.7	52.7	6.6	350.0	.389	212.2	94
October 3, 1981, 1446 UT[d]; Atlantic pass							
Churchill	73.3	20.5	75.5	116.5	0.129	51.0	112
Edmonton	75.2	30.7	76.7	162.0	.179	41.5	46
Goose Bay	58.3	24.9	4.4	380.9	.423	186.1	127
Nashville	56.9	44.1	61.9	142.9	.159	90.8	125
Wallops Island	51.5	40.4	42.2	287.0	.319	136.9	127
White Sands	69.3	53.0	86.2	144.9	.161	64.9	112
October 3, 1981, 1947 UT[d]; Eastern Pacific pass							
Churchill	68.2	57.3	124.4	232.0	0.258	95.7	47
Edmonton	60.5	52.3	122.5	189.8	.211	101.0	117
White Sands	41.1	52.0	94.9	193.3	.215	140.3	101
October 3, 1981, 2047 UT[d]; Eastern Pacific pass							
Churchill	71.7	46.9	107.2	164.4	0.183	65.8	101
Edmonton	63.8	41.1	95.7	134.4	.149	72.7	130
White Sands	45.6	56.4	83.4	184.3	.205	120.9	99

[a] Hourly average for Dobson station location.
[b] Converted from $\overline{C}_2$ using preflight calibration data (eq. (13)).
[c] Number of pixels in a 6° latitude × 6° longitude block centered on the Dobson station location.
[d] Center Universal Time of five SOI 12-minute scenes.

Table 6. SOI Calibration Data and Total Ozone Data at Suitable Dobson Station Locations on September 29 and October 1 to 3, 1981

Station	R	$a_{1,co}$, π unit/unit area	$\bar{s}$	$a_{1,c}$, π unit/unit area	N	Ω, D.U.
September 29, 1981, 1443 UT; Atlantic pass						
Bismarck	0.30	0.170	3.79	0.069	40	283
Boulder	.33	.178	3.95	.073	34	266
Caribou	.57	.331	2.80	.143	64	359
Churchill	.34	.156	3.87	.056	49	(a)
Edmonton	.70	.185	4.20	.057	43	(a)
Goose Bay	.81	.397	2.86	.178	69	(a)
Toronto	.49	.295	2.96	.137	55	307
Wallops Island	.11	.223	2.85	.110	57	302
White Sands	.15	.175	4.05	.070	31	278
September 29, 1981, 2118 UT; Eastern Pacific pass						
Bismarck	0.49	0.295	3.34	.136	103	281
Boulder	.37	.290	3.19	.140	106	265
Churchill	.14	.158	4.09	.053	95	(a)
Edmonton	.72	.317	3.34	.121	96	350
Toronto	.19	.195	4.57	.060	106	(a)
White Sands	.22	.283	3.18	.138	109	262
September 29, 1981, 2218 UT; Eastern Pacific pass						
Bismarck	0.54	0.223	3.97	0.089	101	282
Boulder	.47	.263	3.75	.112	104	280
Churchill	.12	.110	4.55	.033	94	(a)
Edmonton	.71	.232	3.87	.076	95	(a)
Toronto	.47	.167	5.04	.045	104	(a)
White Sands	.33	.283	3.62	.124	106	268
October 1, 1981, 1424 UT; Atlantic pass						
Bismarck	0.39	0.163	4.04	0.061	37	(a)
Boulder	.11	.130	4.16	.051	33	(a)
Caribou	.34	.241	2.81	.116	61	(a)
Churchill	.15	.111	4.11	.036	47	(a)
Edmonton	.64	.155	4.43	.054	41	(a)
Goose Bay	.51	.273	2.87	.128	67	328
Toronto	.84	.389	3.02	.149	51	(a)
Wallops Island	.47	.314	2.85	.157	54	(a)
White Sands	.60	.219	4.23	.083	29	296

[a]Excluded because rain conditions existed at ground station or $\theta_0 > 70°$.

Table 6. Continued

Station	R	$a_{1,co}$, π unit/unit area	$\bar{s}$	$a_{1,c}$, π unit/unit area	N	Ω, D.U.
October 1, 1981, 1524 UT; Atlantic pass						
Bismarck	0.42	0.228	3.50	0.097	48	321
Boulder	.14	.178	3.59	.079	44	269
Caribou	.37	.291	2.94	.135	72	(a)
Churchill	.19	.144	3.64	.053	55	321
Edmonton	.70	.201	4.05	.076	47	(a)
Goose Bay	.53	.302	2.99	.137	76	331
Toronto	.85	.466	3.00	.199	62	(a)
Wallops Island	.49	.376	2.99	.182	66	298
White Sands	.66	.330	3.73	.141	40	287
October 1, 1981, 1951 UT; Eastern Pacific pass						
Bismarck	0.08	0.291	3.32	0.130	114	301
Boulder	.03	.252	3.06	.126	116	285
Churchill	.08	.240	3.92	.081	102	330
Edmonton	.41	.325	3.44	.136	102	317
White Sands	.44	.396	2.86	.206	117	276
October 1, 1981, 2051 UT; Eastern Pacific pass						
Bismarck	0.14	0.228	3.31	0.102	104	310
Boulder	.08	.216	3.14	.106	107	295
Churchill	.11	.170	4.04	.056	96	(a)
Edmonton	.44	.251	3.34	.108	96	298
Toronto	.78	.265	4.58	.072	106	(a)
White Sands	.46	.379	3.11	.186	110	277
October 2, 1981, 1628 UT; North America pass						
Bismarck	0.03	0.234	2.94	0.115	58	307
Boulder	.24	.291	2.94	.151	47	259
Churchill	.23	.265	3.44	.111	68	324
Edmonton	.58	.314	3.45	.128	53	312
Goose Bay	.42	.362	3.34	.146	103	(a)
Nashville	.05	.283	2.62	.143	79	324
Toronto	.56	.436	2.73	.197	89	360
Wallops Island	.50	.437	2.57	.212	98	(a)
White Sands	.48	.384	2.76	.206	39	(a)

[a]Excluded because rain conditions existed at ground station or $\theta_0 > 70°$

Table 6. Concluded

Station	R	$a_{1,co}$, π unit/unit area	$\bar{s}$	$a_{1,c}$, π unit/unit area	N	Ω, D.U.
October 2, 1981, 1728 UT; North America pass						
Bismarck	0.04	0.180	2.65	0.095	71	306
Boulder	.25	.250	2.57	.141	68	278
Churchill	.23	.198	3.08	.091	75	337
Edmonton	.64	.304	2.98	.135	66	311
Goose Bay	.45	.276	3.19	.116	97	(a)
Nashville	.08	.232	2.52	.121	87	311
Toronto	.60	.400	2.67	.184	90	361
Wallops Island	.55	.404	2.66	.181	96	(a)
White Sands	.48	.368	2.53	.209	67	(a)
October 2, 1981, 1828 UT; North America pass						
Bismarck	0.08	0.204	2.82	0.106	81	296
Boulder	.31	.292	2.79	.156	79	273
Churchill	.28	.199	3.15	.083	80	321
Edmonton	.62	.316	2.97	.139	75	(a)
Goose Bay	.46	.232	3.55	.088	96	(a)
Nashville	.09	.259	2.92	.121	92	308
Toronto	.66	.406	2.99	.170	94	364
Wallops Island	.57	.399	3.08	.159	98	(a)
White Sands	.45	.396	2.88	.208	79	(a)
October 3, 1981, 1446 UT; Atlantic pass						
Churchill	0.34	0.185	3.99	0.049	(a)	(a)
Edmonton	.66	.168	4.33	.050	(a)	(a)
Goose Bay	.80	.392	2.92	.180	(a)	(a)
Nashville	.06	.206	3.13	.093	(a)	(a)
Wallops Island	.44	.319	2.89	.143	(a)	(a)
White Sands	.21	.184	4.04	.072	(a)	(a)
October 3, 1981, 1947 UT; Eastern Pacific pass						
Churchill	0.31	0.272	4.00	0.099	102	319
Edmonton	.05	.258	3.47	.096	102	330
White Sands	.09	.269	2.89	.137	118	(a)
October 3, 1981, 2047 UT; Eastern Pacific pass						
Churchill	0.31	0.190	4.11	0.068	96	(a)
Edmonton	.08	.185	3.38	.071	97	337
White Sands	.12	.254	3.13	.122	111	(a)

[a]Excluded because rain conditions existed at ground station or $\theta_0 > 70°$.

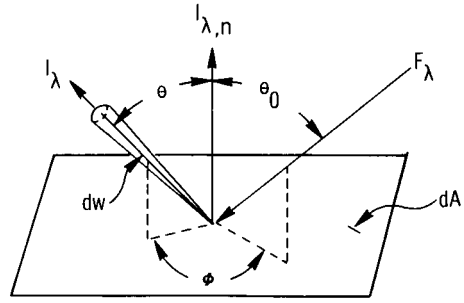

F_λ = Solar flux over a wavelength interval assumed parallel through the atmosphere at the earth distance from the sun

$I_{\lambda,n}$ = F_λ diffusely scattered normal to dA into a hemisphere per unit time, per unit frequency, per unit solid angle

I_λ = Energy diffusely scattered into a hemisphere in a direction θ from $I_{\lambda,n}$ per unit time, per unit frequency, per unit solid angle (dw)

Figure 1. Diagram illustrating incident solar flux and scattering angles.

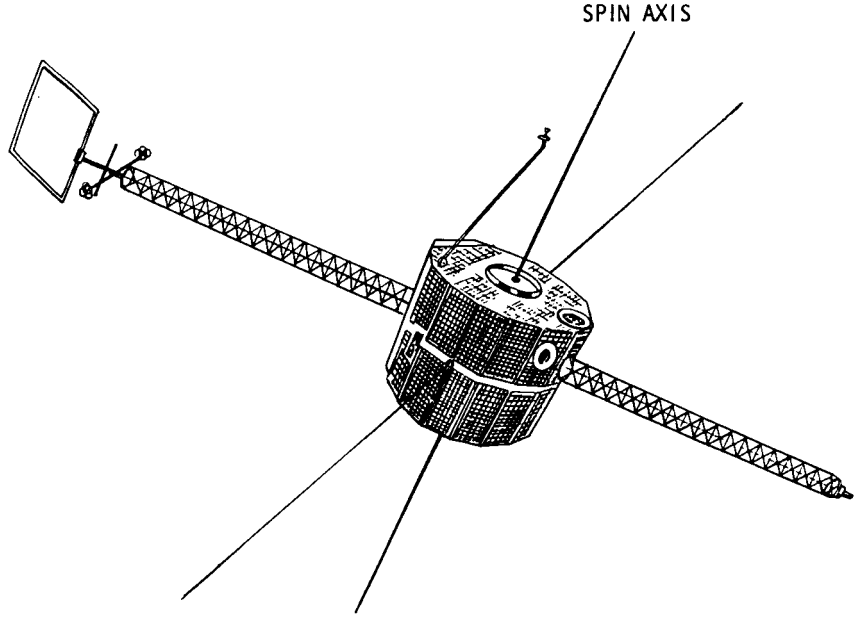

Figure 2. Sketch of the Dynamics Explorer 1 spacecraft.

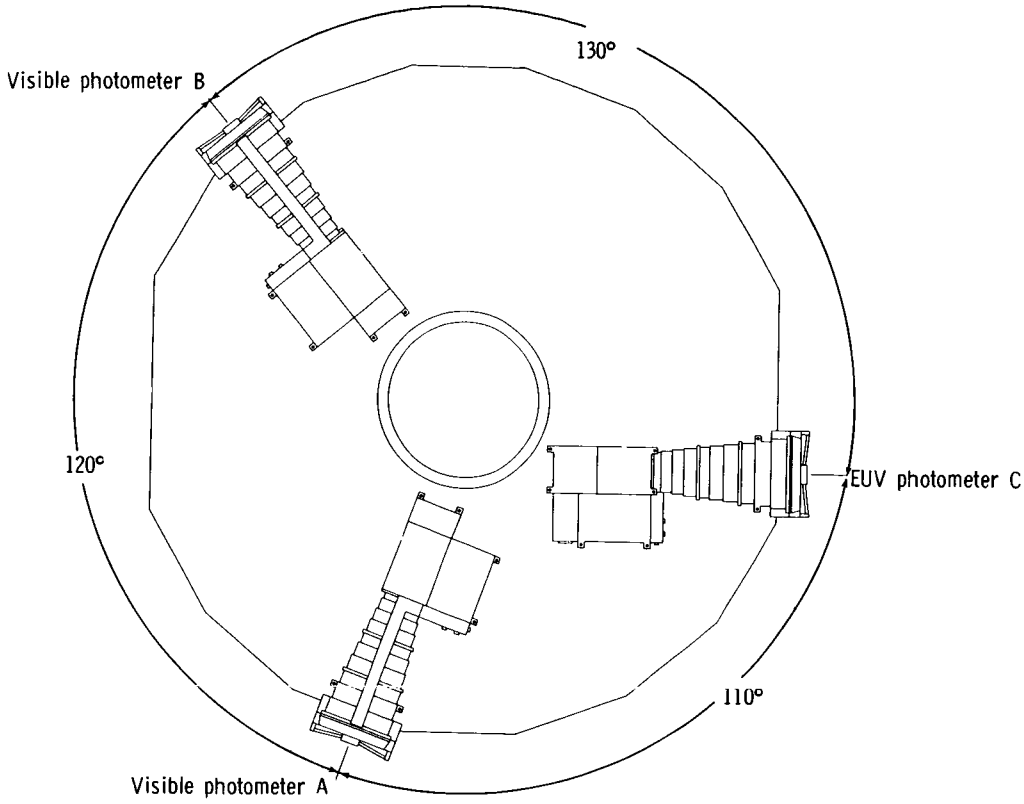

Figure 3. Location of the three photometers aboard Dynamics Explorer 1.

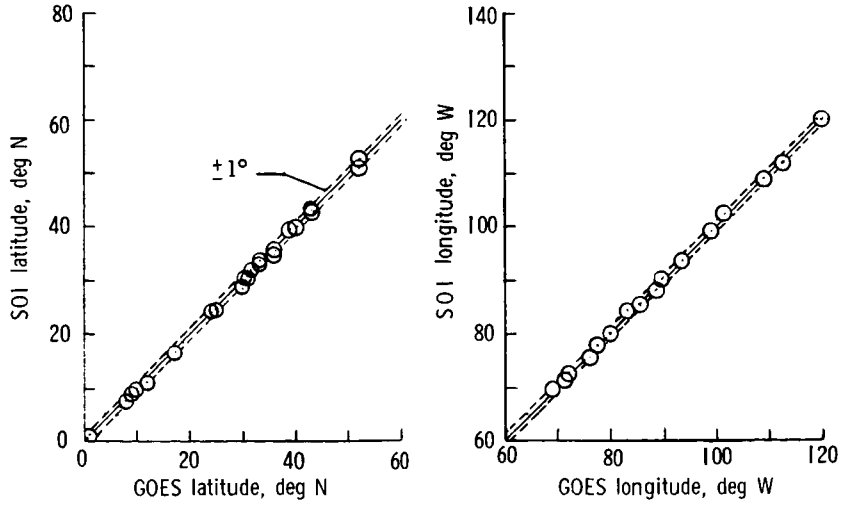

Figure 4. Location of identical cloud edges from SOI and GOES scenes.

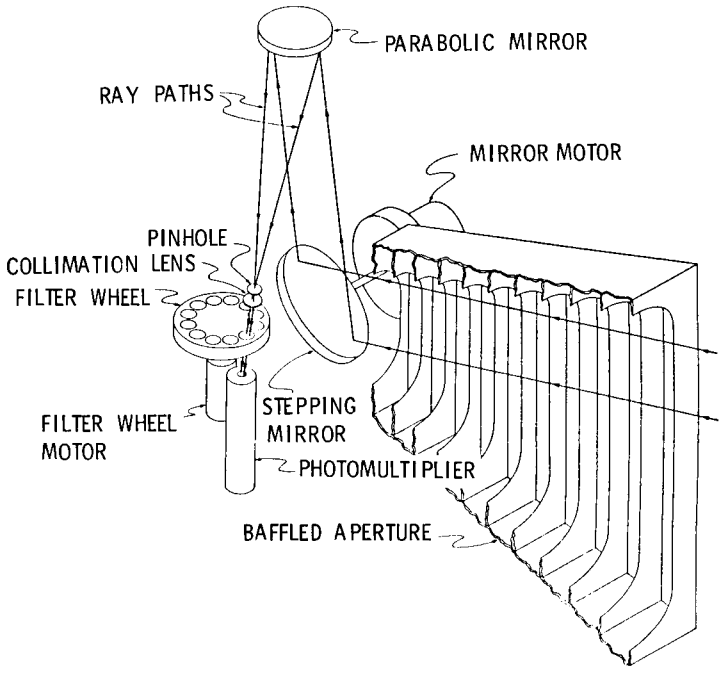

Figure 5. Schematic of a DE-1 photometer.

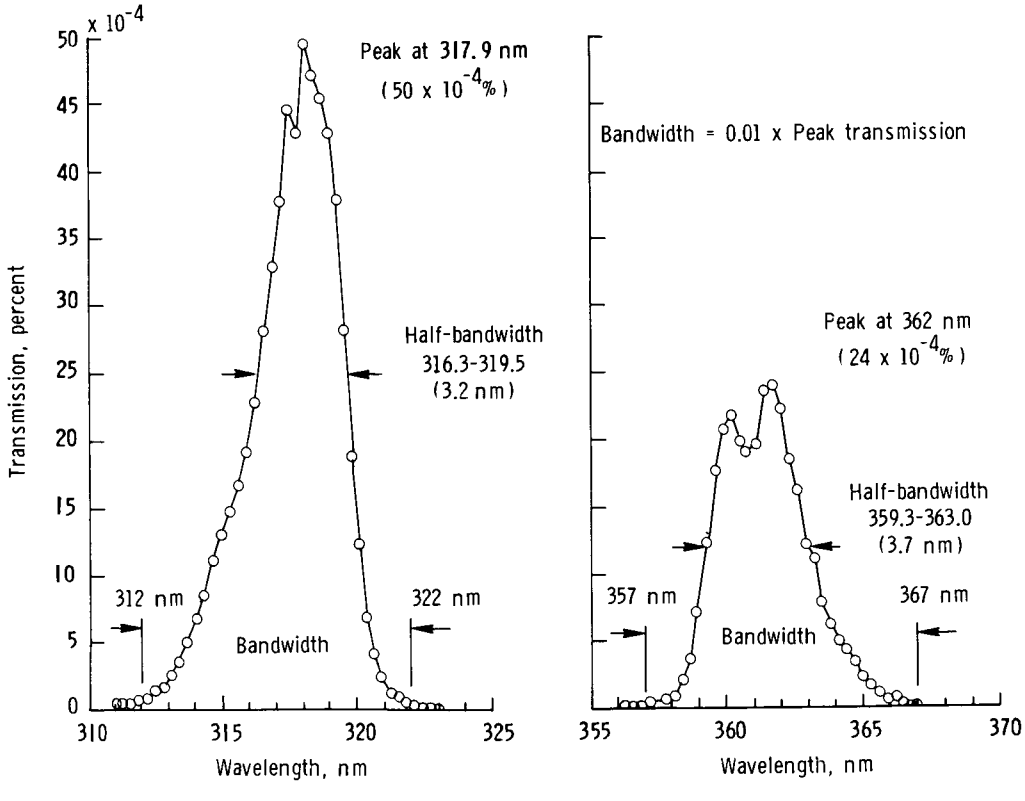

(a) 317.5-nm filter; Temperature = 15.3°C.

(b) 360-nm filter; Temperature = 14.5°C.

Figure 6. Transmission versus wavelength for the SOI optical filters.

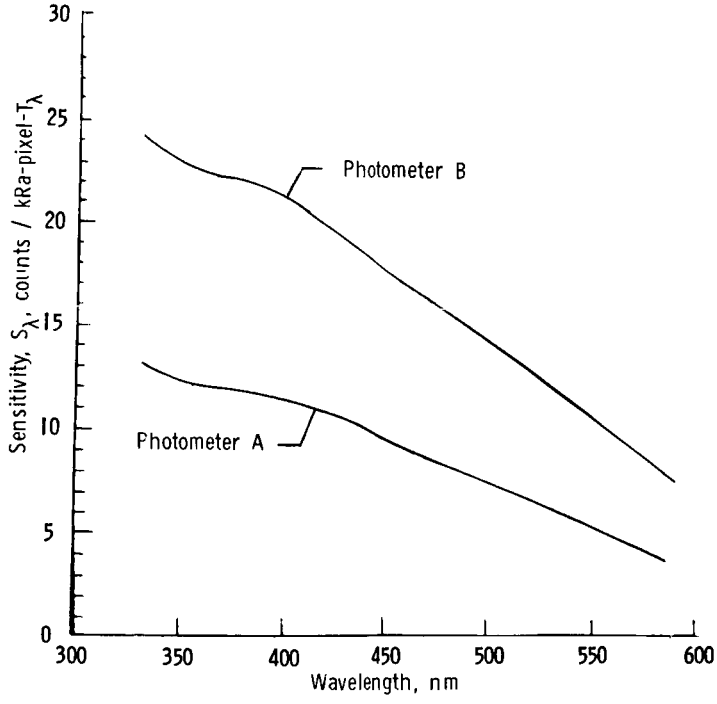

Figure 7. Sensitivity of photometers A and B versus wavelength.

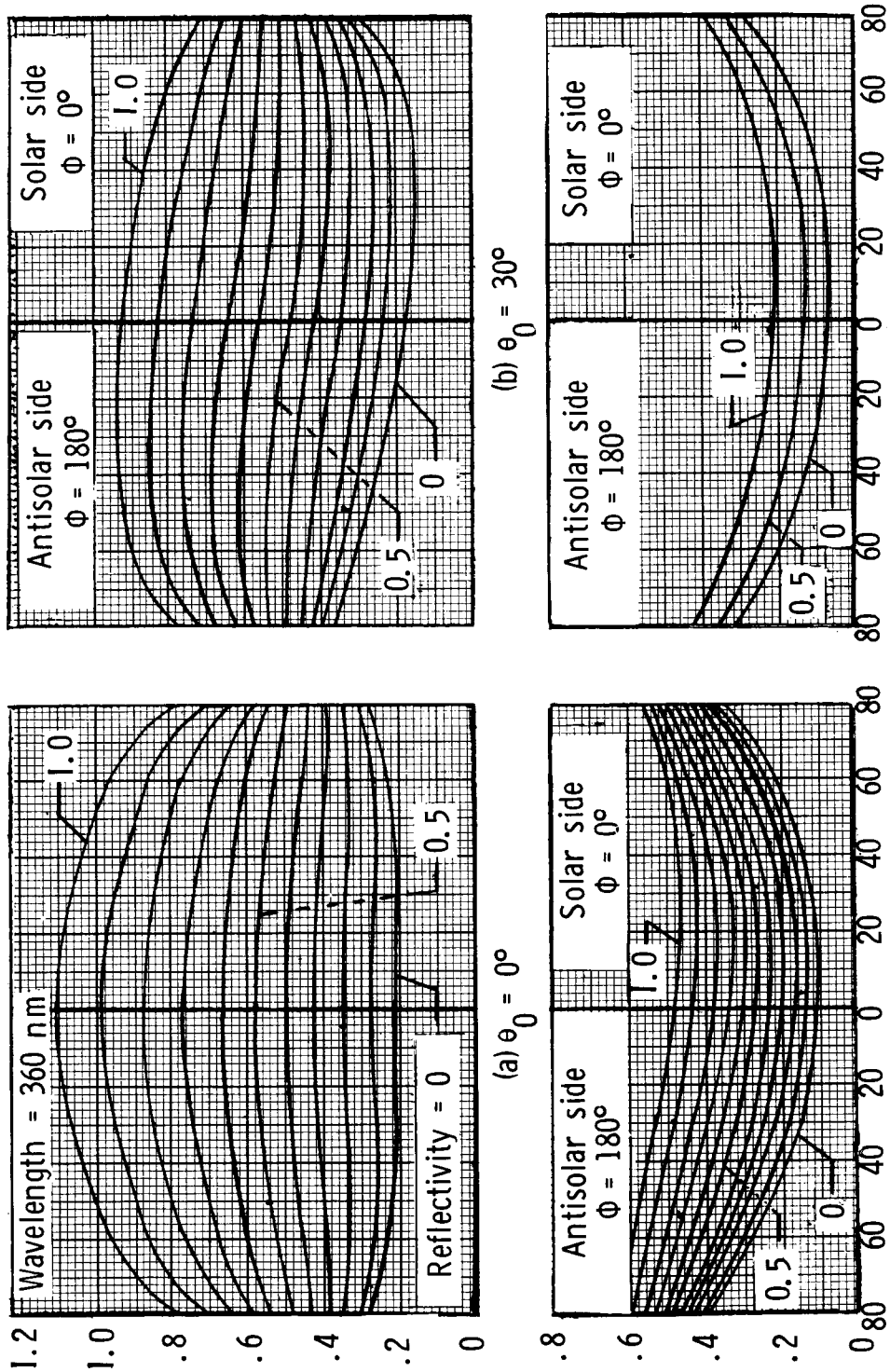

Figure 8. Theoretical albedo at 360 nm, $a_{2,c}$, in the plane of the Sun versus reflectivity and view angle.

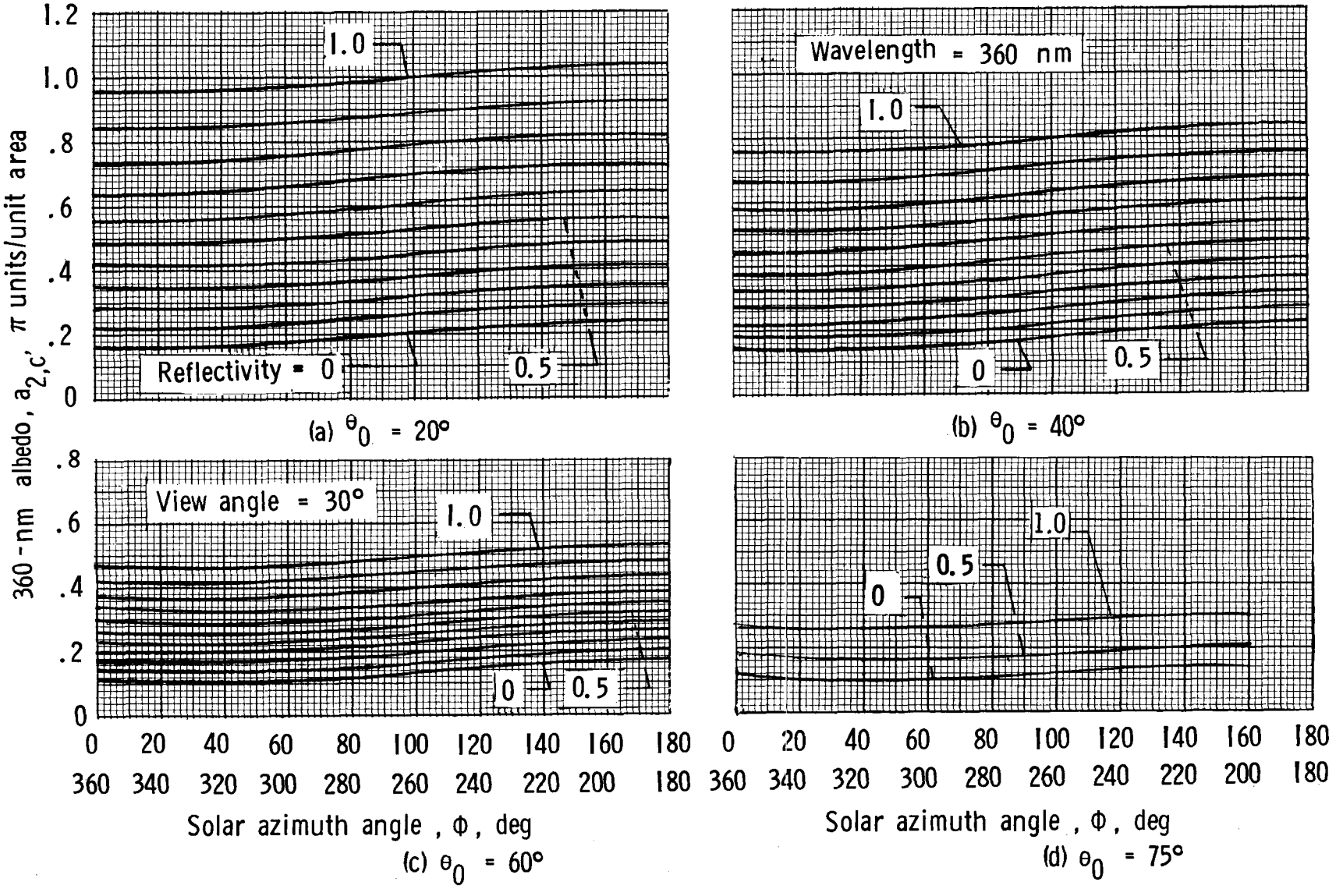

Figure 9. Theoretical albedo at 360 nm, $a_{2,c}$, for a view angle θ of 30° versus reflectivity and solar azimuth angle.

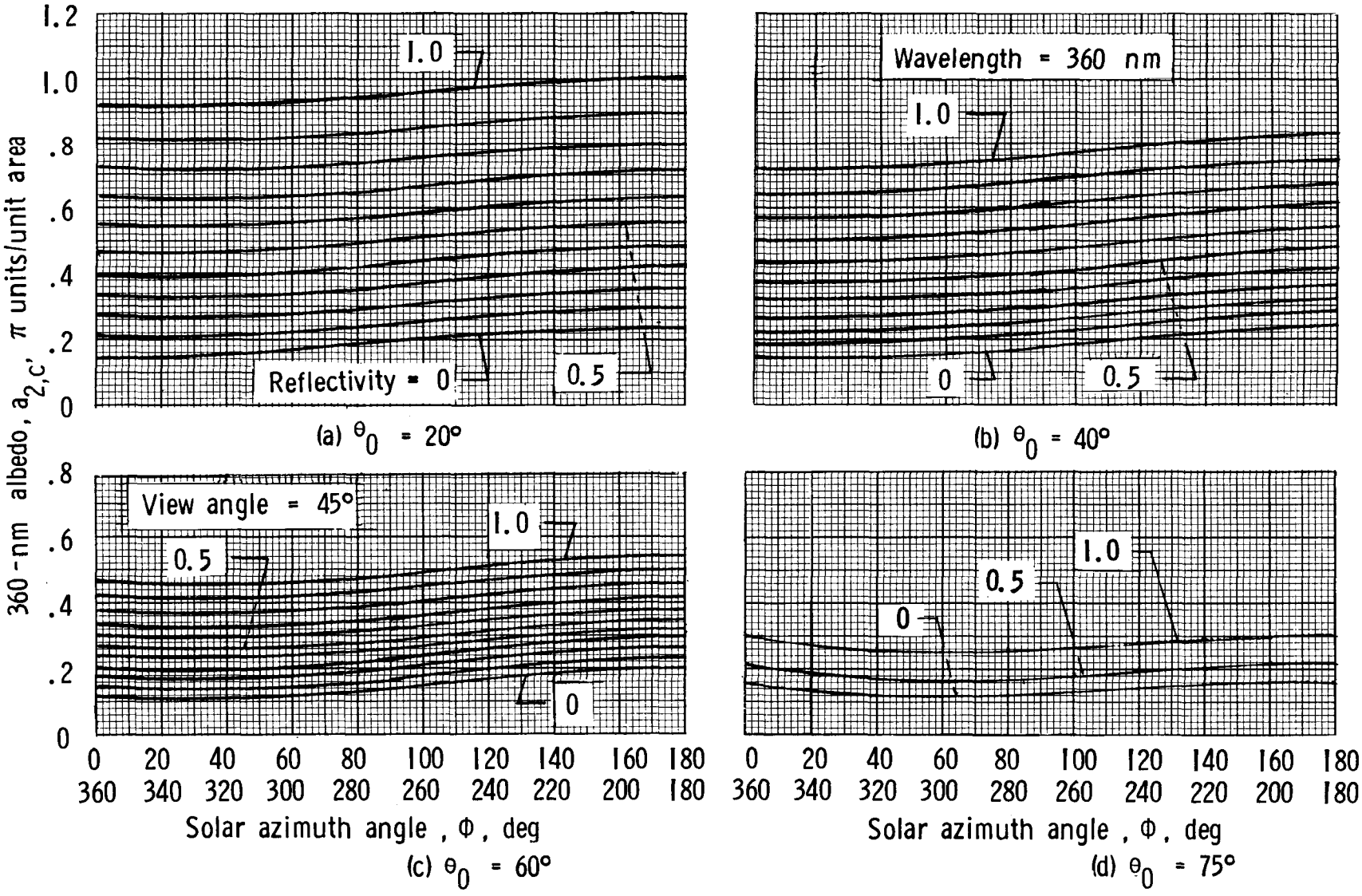

Figure 10. Theoretical albedo at 360 nm, $a_{2,c}$, for a view angle θ of 45° versus reflectivity and solar azimuth angle.

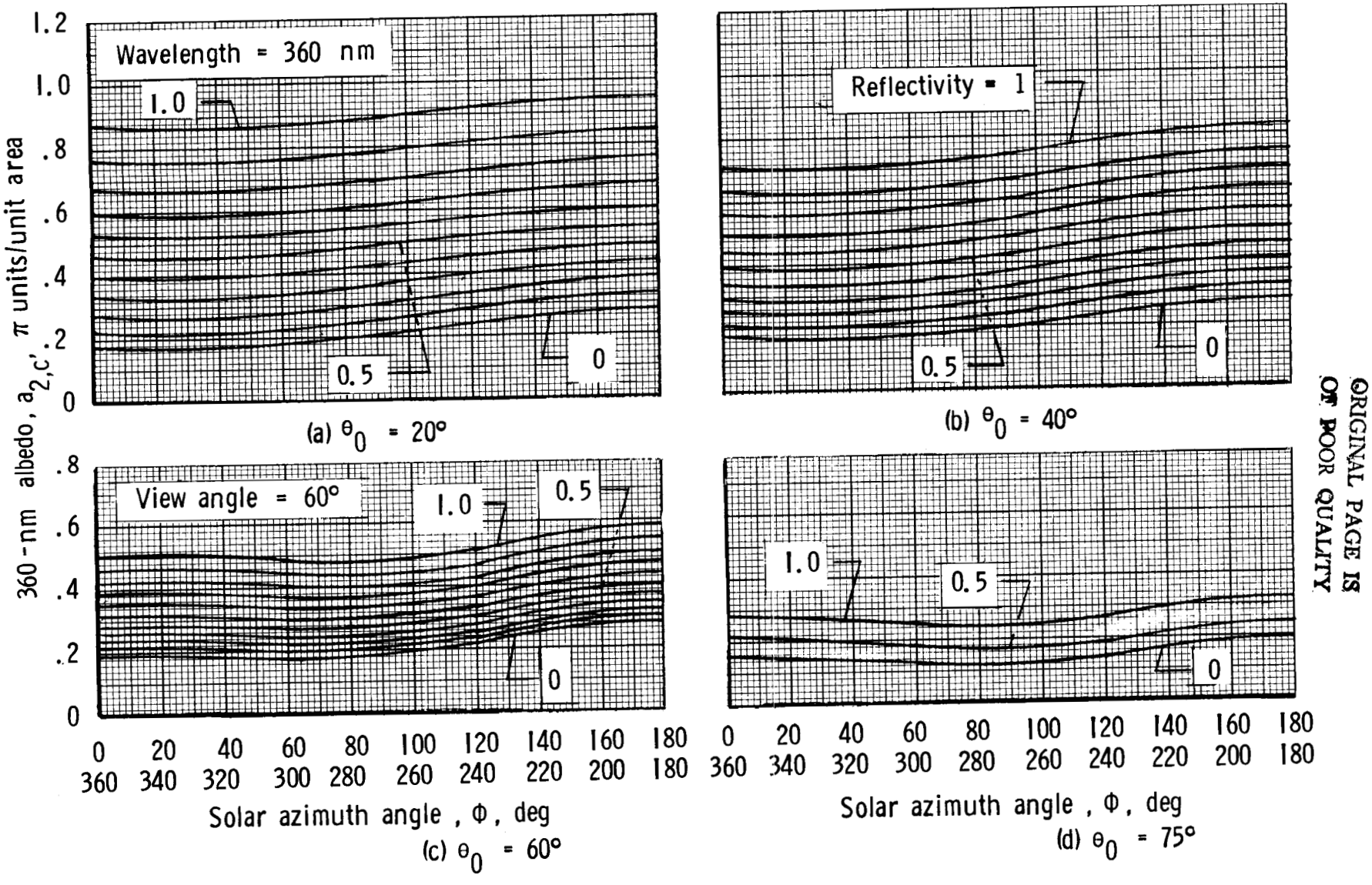

Figure 11. Theoretical albedo at 360 nm, $a_{2,c}$, for a view angle θ of 60° versus reflectivity and solar azimuth angle.

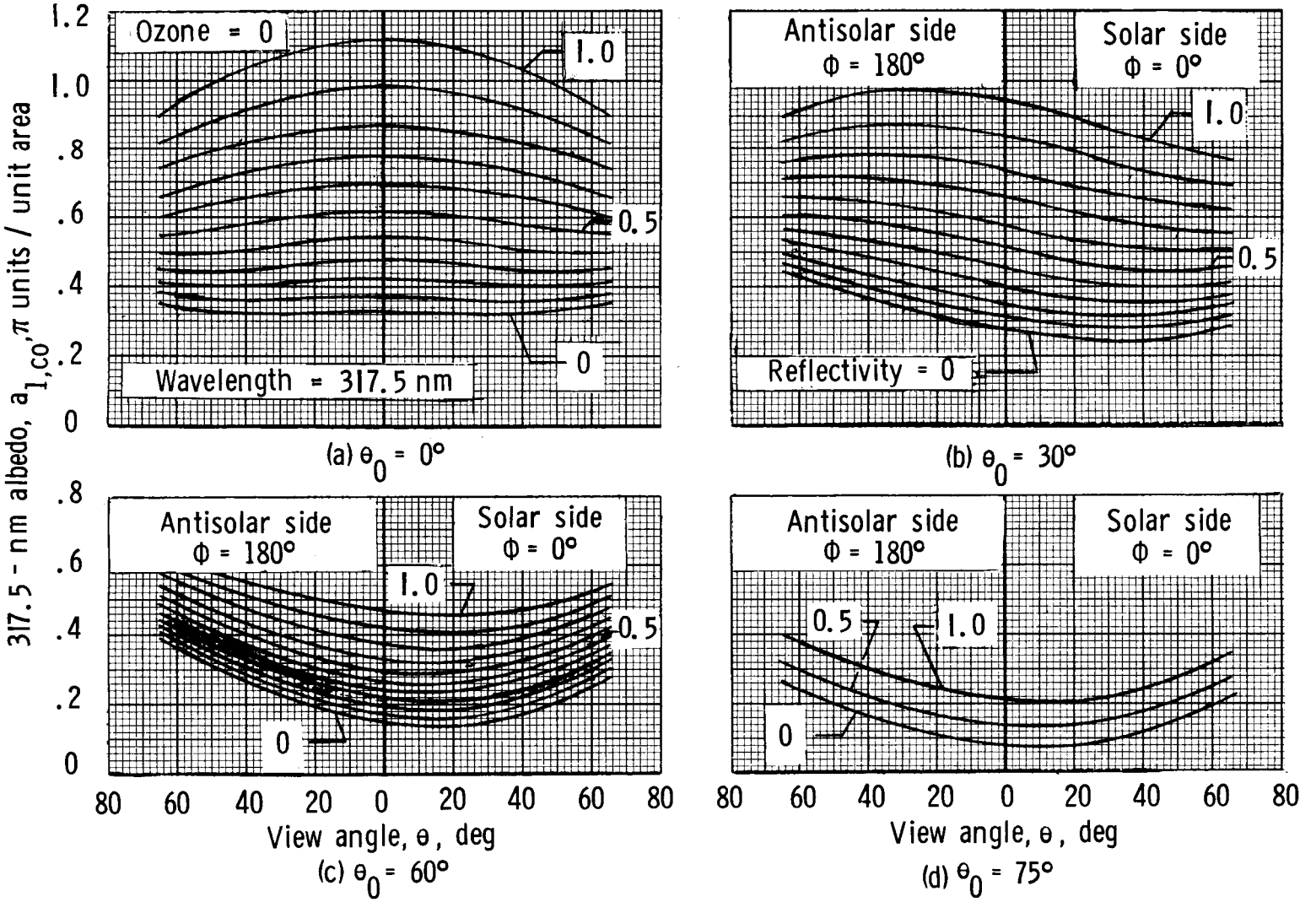

Figure 12. Theoretical albedo at 317.5 nm without ozone, $a_{1,co}$, in the plane of the Sun versus reflectivity and view angle.

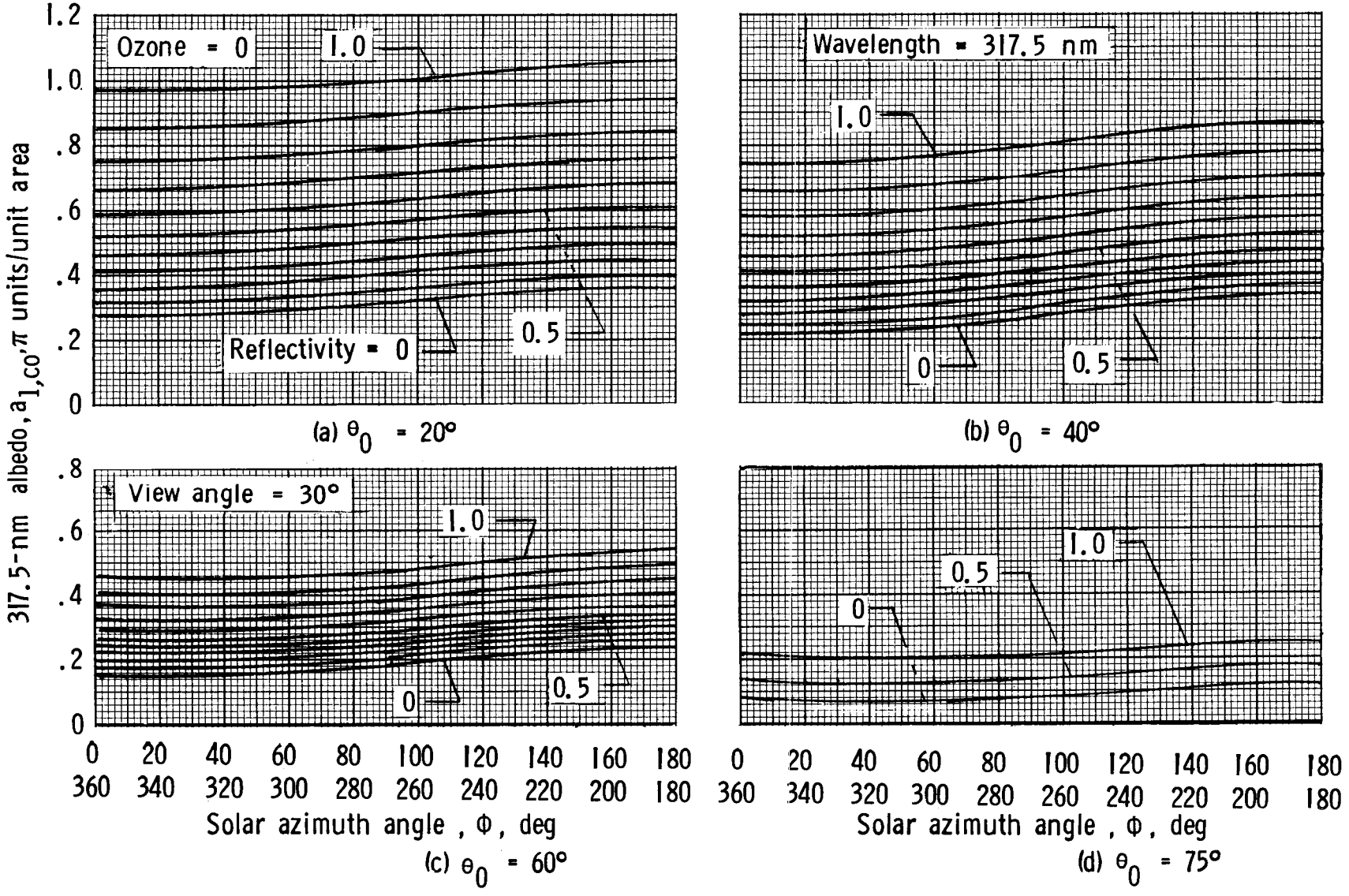

Figure 13. Theoretical albedo at 317.5 nm without ozone, $a_{1,co}$, for a view angle θ of 30° versus reflectivity and solar azimuth angle.

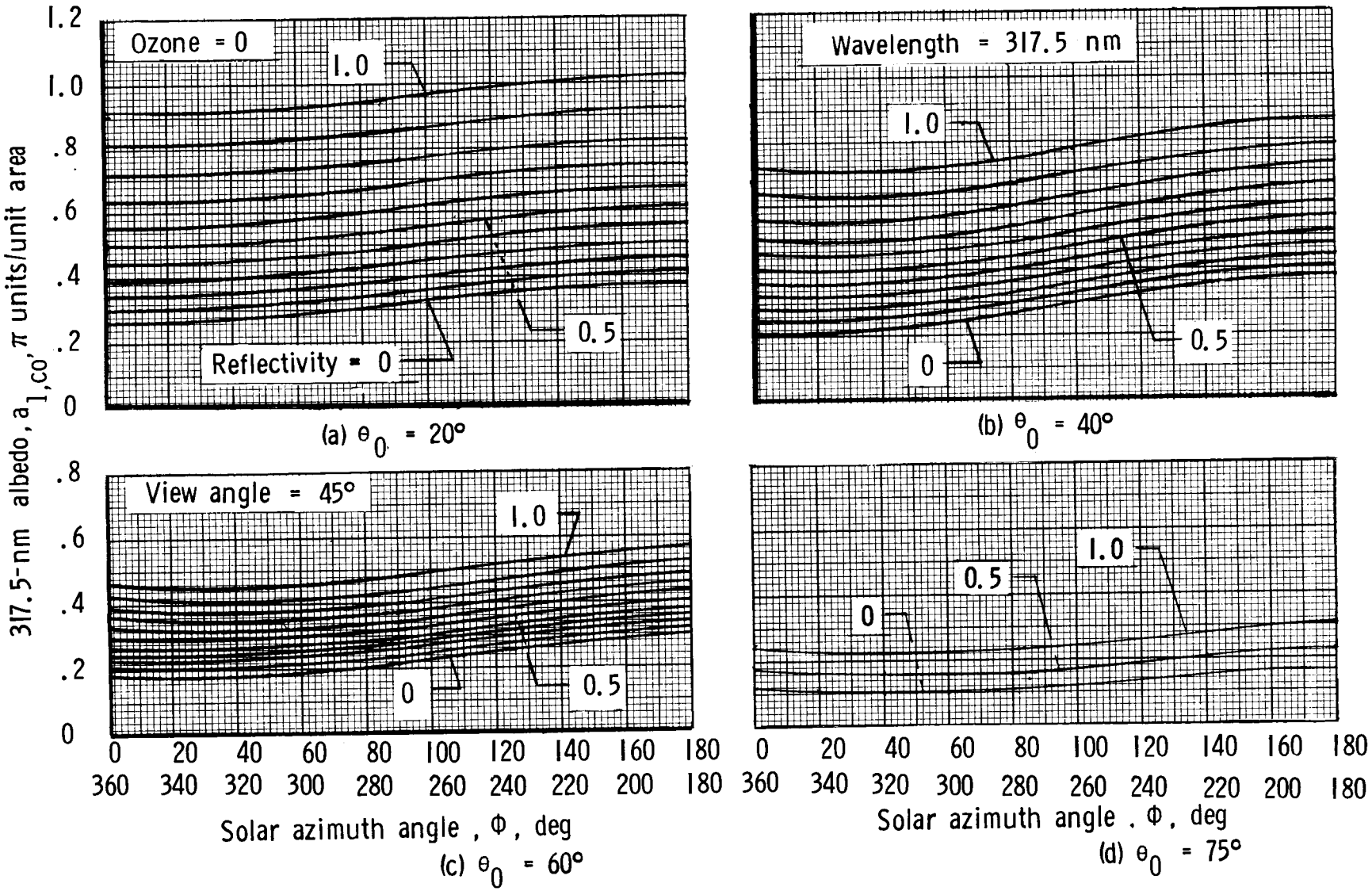

Figure 14. Theoretical albedo at 317.5 nm without ozone, $a_{1,co}$, for a view angle θ of 45° versus reflectivity and solar azimuth angle.

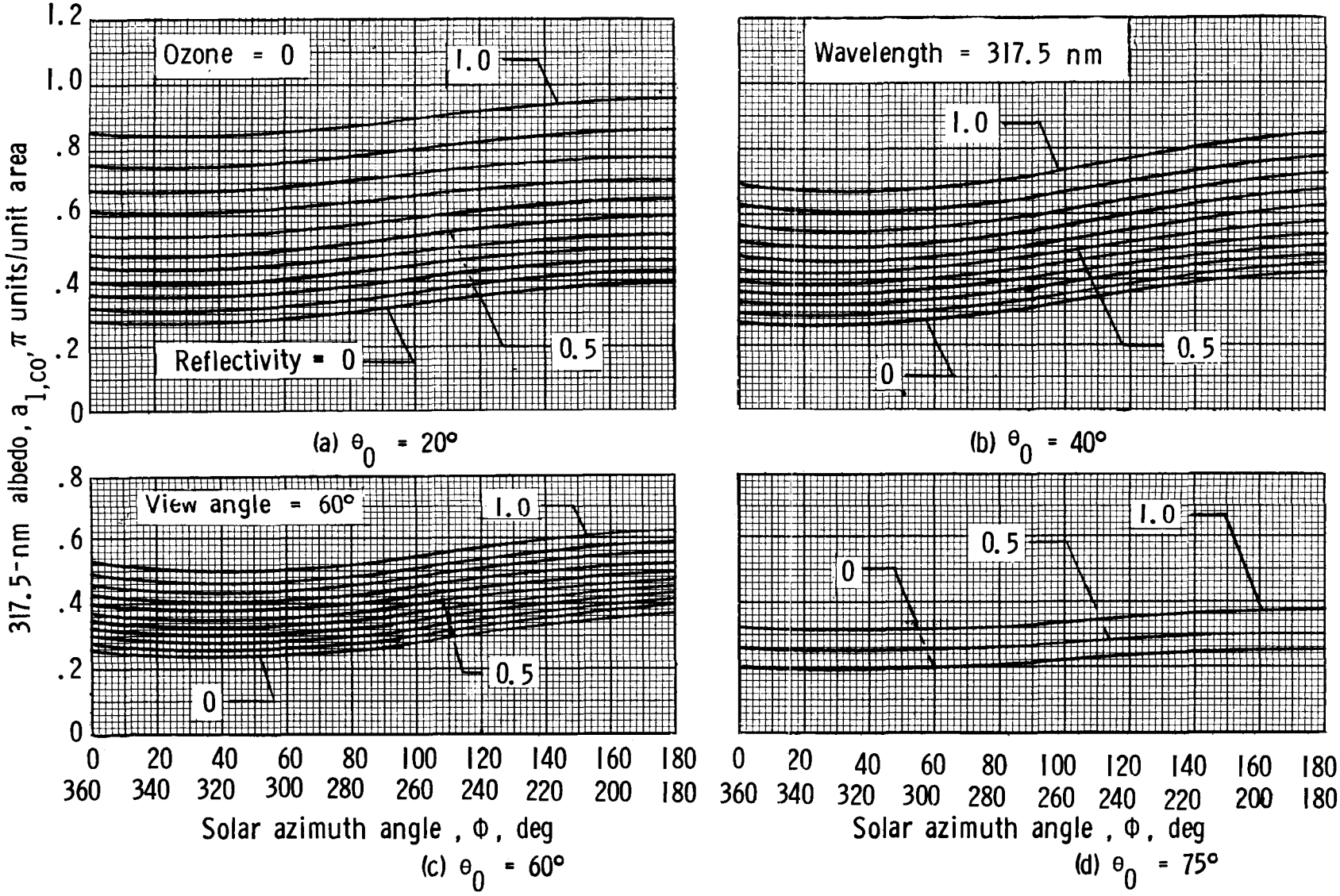

Figure 15. Theoretical albedo at 317.5 nm without ozone, $a_{1,co}$, for a view angle θ of 60° versus reflectivity and solar azimuth angle.

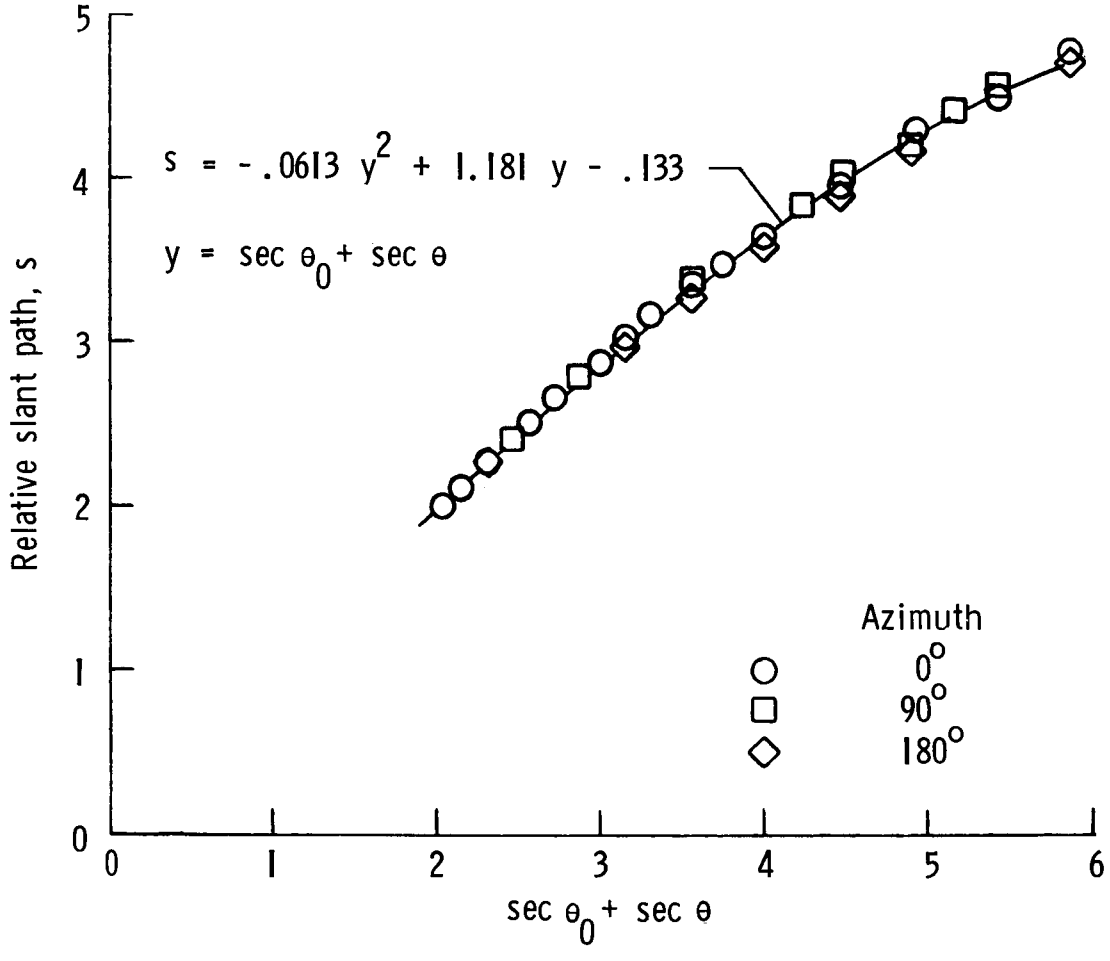

Figure 16. Calculated relative slant path versus the sum of the secants of solar zenith and view angles.

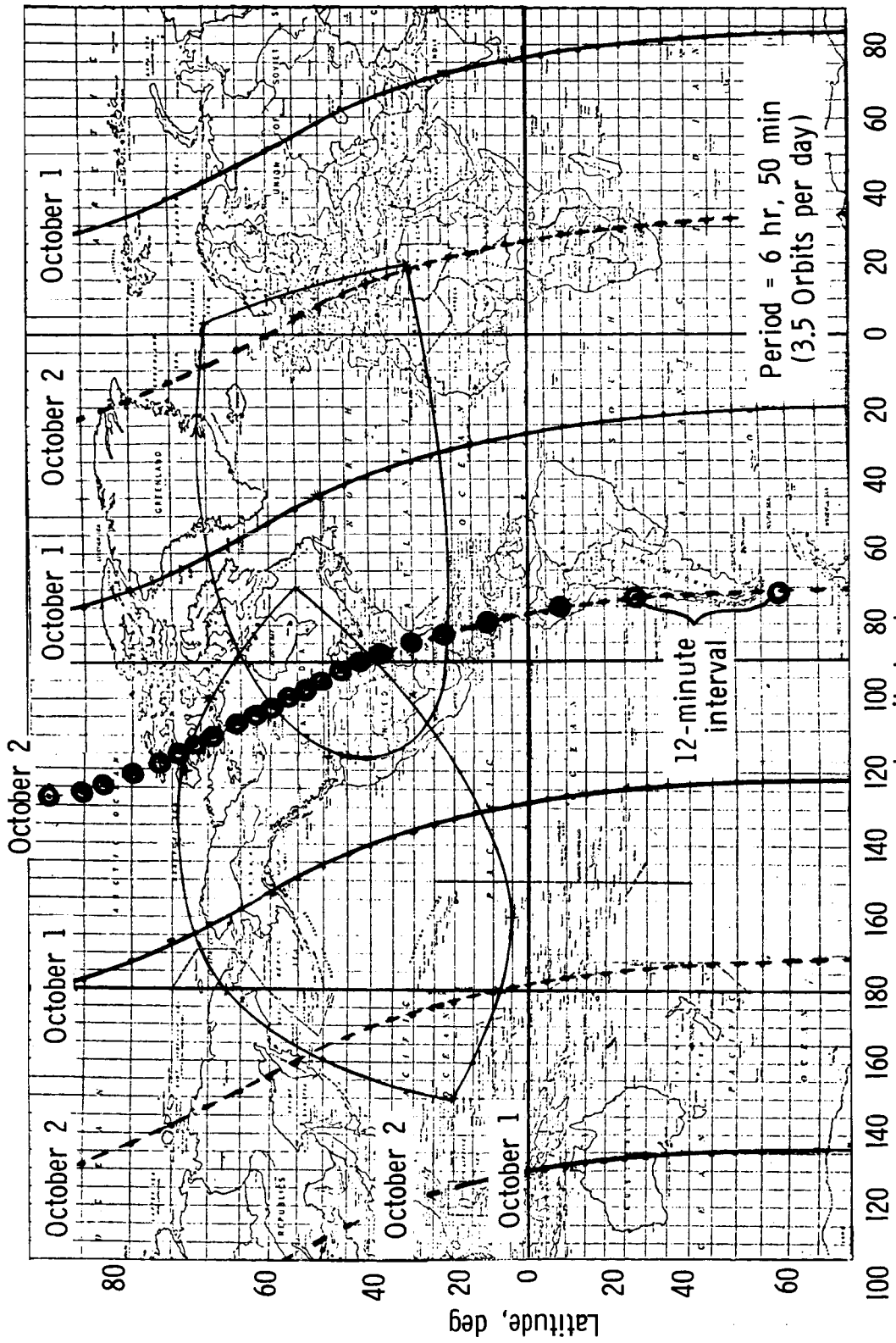

Figure 17. The Earth track of DE-1 on October 1 and 2, 1981, showing the location of the center and the number of SOI scenes obtained over North and South America on October 2, 1981, and the extent of a North Atlantic and an eastern Pacific Ocean scene.

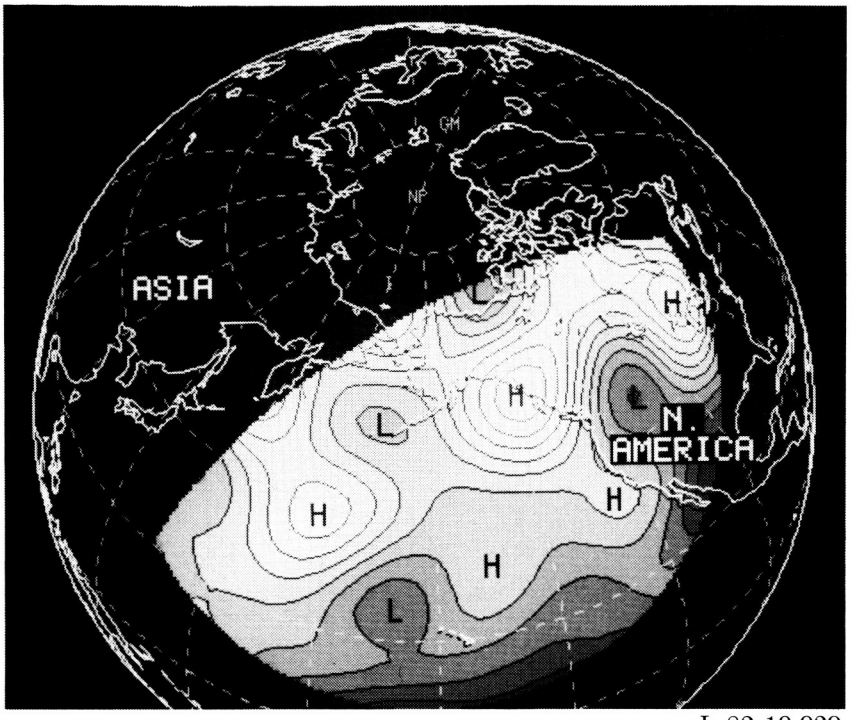

L-82-10,929

Figure 18. Total ozone contour map over the eastern Pacific Ocean from SOI radiance data on October 1, 1981. High ozone is designated by H and low by L with the contour lines varying between 250 and 380 D.U.

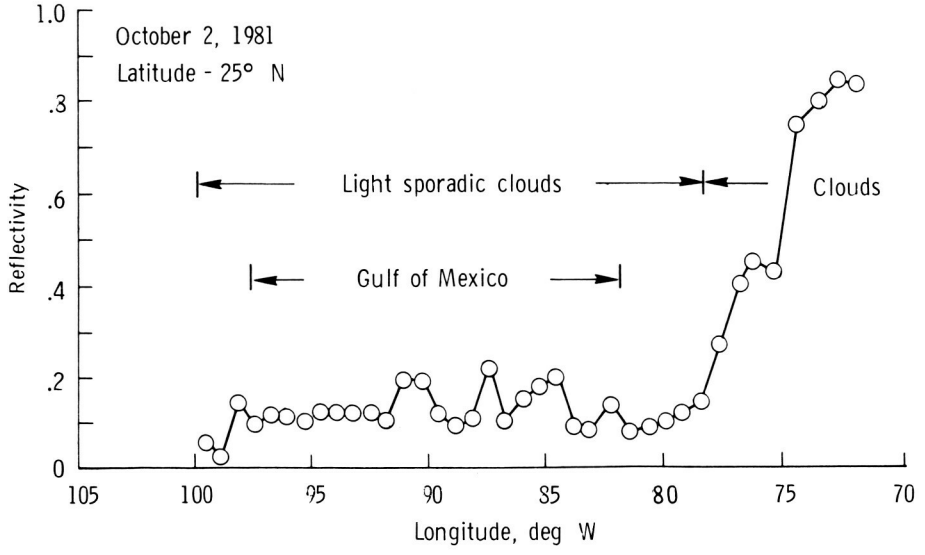

Figure 19. Calculated reflectivity from the SOI 360-nm radiance measurements between longitude 71.9° and 99.5° west along 25° north latitude on October 2, 1981, at 17:16 UT.

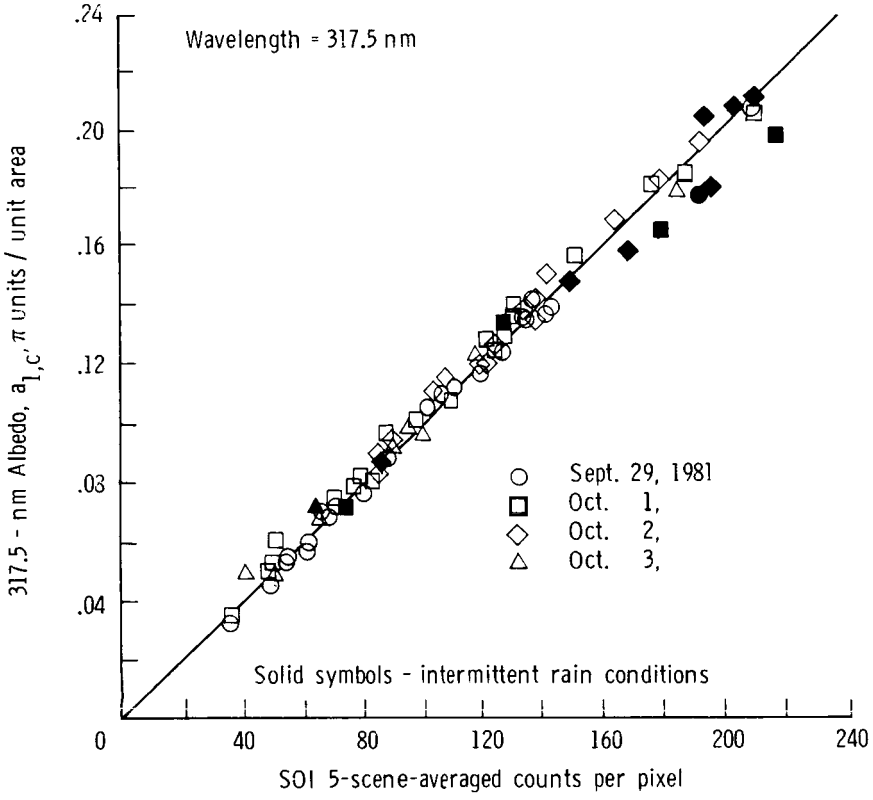

Figure 20. Calculated 317.5-nm albedo from Dobson station total ozone data versus SOI five-scene-averaged counts per pixel on September 29, and October 1, 2, and 3, 1981.

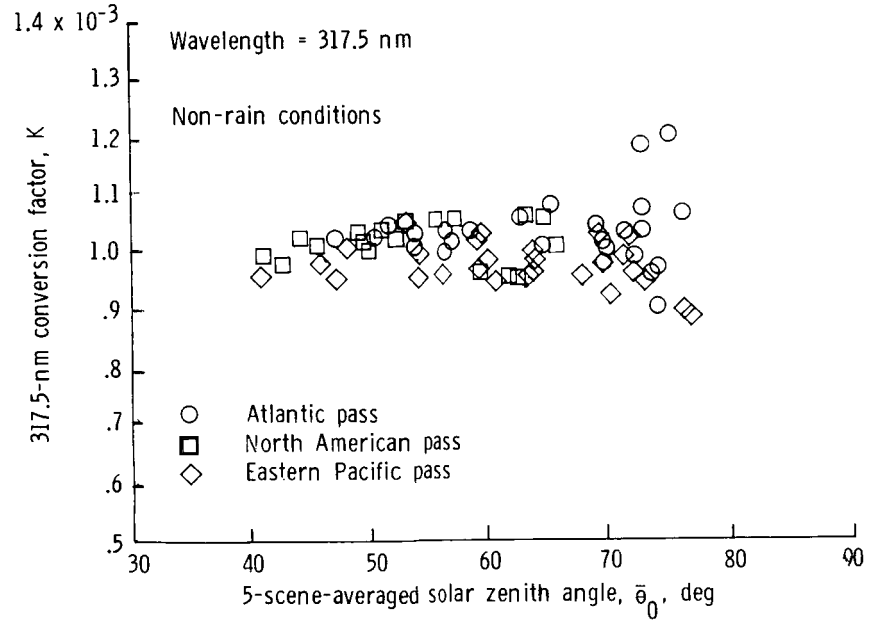

Figure 21. The 317.5-nm conversion factor versus five-scene-averaged solar zenith angle, at Dobson station locations from Atlantic, North American, and Pacific orbital passes.

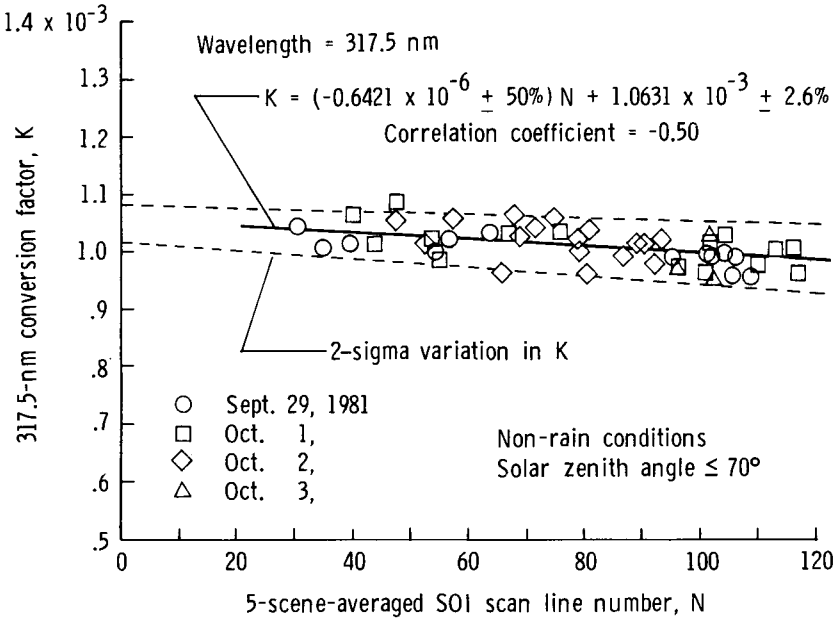

Figure 22. The SOI 317.5-nm conversion factor versus SOI average scan line number that included the Dobson station location on September 29 and October 1, 2, and 3, 1981.

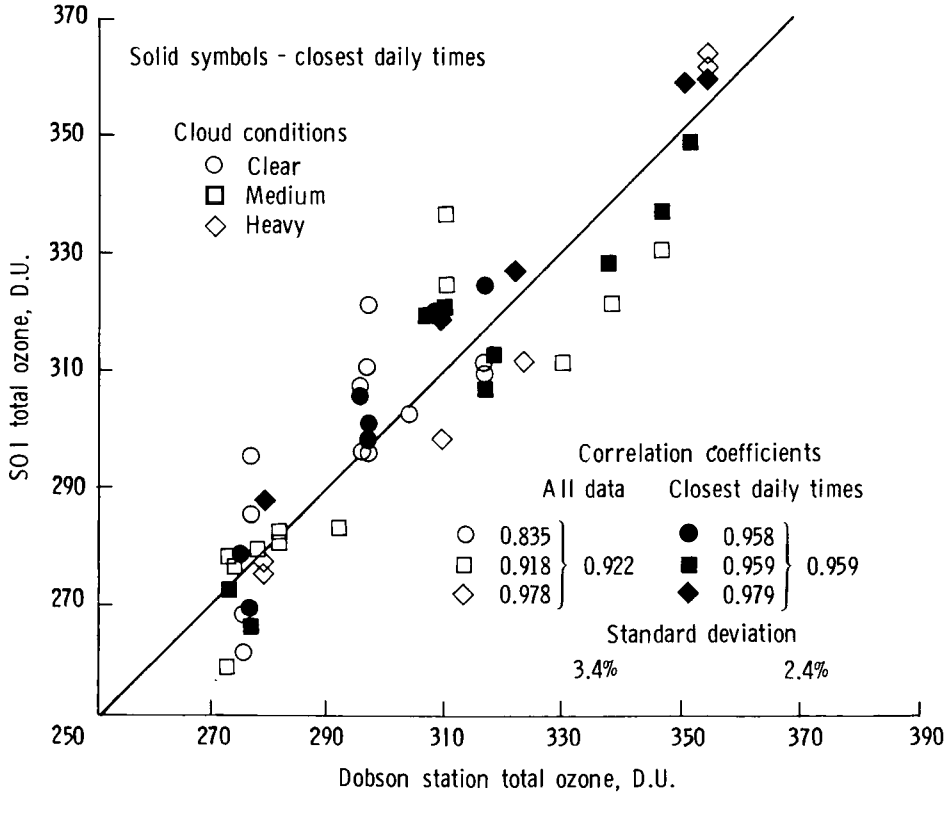

Figure 23. SOI total ozone versus Dobson station total ozone for September 29 and October 1, 2, and 3, 1981, for clear, medium, and heavy cloud conditions.

NASA
National Aeronautics and Space Administration

Report Documentation Page

1. Report No.	2. Government Accession No.	3. Recipient's Catalog No.
NASA TP-2723		

4. Title and Subtitle	5. Report Date
Calibration of the Spin-Scan Ozone Imager Aboard the Dynamics Explorer 1 Satellite	August 1987
	6. Performing Organization Code
7. Author(s)	8. Performing Organization Report No.
Walter E. Bressette, Gerald M. Keating and David F. Young	L-16150
9. Performing Organization Name and Address	10. Work Unit No.
NASA Langley Research Center Hampton, VA 23665-5225	675-41-07-02
	11. Contract or Grant No.
12. Sponsoring Agency Name and Address	13. Type of Report and Period Covered
National Aeronautics and Space Administration Washington, DC 20546-0001	Technical Paper
	14. Sponsoring Agency Code

15. Supplementary Notes

Walter E. Bressette and Gerald M. Keating: Langley Research Center, Hampton, Virginia.
David F. Young: ST Systems Corporation (STX), Hampton, Virginia.

16. Abstract

This paper presents the calibration technique, contains calculated backscattered radiance values necessary for performing the calibrations, and provides the calibration constants for September–October 1981 to determine total columnar ozone from the Spin-Scan Ozone Imager (SOI), which is a part of the auroral imaging instrumentation aboard the Dynamics Explorer 1 Satellite. The precision of the SOI-derived total columnar ozone is estimated to be better than 2.4 percent. Linear regression analysis was used to calculate correlation coefficients between total columnar ozone obtained from Dobson ground stations and SOI which indicate that the SOI total columnar ozone determination is equally accurate for clear or cloudy weather conditions.

17. Key Words (Suggested by Authors(s))	18. Distribution Statement
Ozone Satellite calibration Meteorology Atmospheric albedo Total ozone algorithmn	Unclassified—Unlimited Subject Category 47

19. Security Classif.(of this report)	20. Security Classif.(of this page)	21. No. of Pages	22. Price
Unclassified	Unclassified	43	A03

NASA-Langley, 1987
For sale by the National Technical Information Service, Springfield, Virginia 22161-2171